



Published in final edited form as:

Cell Rep. 2020 April 07; 31(1): 107249. doi:10.1016/j.celrep.2020.01.040.

TLR9 Sensing of Self-DNA Controls Cell-Mediated Immunity to *Listeria* Infection via Rapid Conversion of Conventional CD4⁺ T Cells to T_{reg}

Joseph S. Dolina^{1,8,*}, Joey Lee¹, Ryan Q. Griswold¹, Lara Labarta-Bajo^{1,2}, Sumetha Kannan³, Jason A. Greenbaum³, Nawal Bahia El Idrissi^{1,4}, Margot J. Pont^{1,5}, Michael Croft^{6,7}, Stephen P. Schoenberger^{1,*}

¹Division of Developmental Immunology, La Jolla Institute for Immunology, La Jolla, CA 92037, USA

²Section of Molecular Biology, University of California, San Diego, La Jolla, CA 92093, USA

³Bioinformatics Core, La Jolla Institute for Immunology, La Jolla, CA 92037, USA

⁴Department of Neurogenetics, Academic Medical Center, Amsterdam, the Netherlands

⁵Clinical Research Division, Fred Hutchinson Cancer Research Center, Seattle, WA 98109, USA

⁶Division of Immune Regulation, La Jolla Institute for Immunology, La Jolla, CA 92037, USA

⁷Department of Medicine, University of California, San Diego, La Jolla, CA 92093, USA

⁸Lead Contact

SUMMARY

CD4⁺ T lymphocytes are crucial for controlling a range of innate and adaptive immune effectors. For CD8⁺ cytotoxic T lymphocyte (CTL) responses, CD4⁺ T cells can function as helpers (T_H) to amplify magnitude and functionality or as regulatory cells (T_{reg}) capable of profound inhibition. It is unclear what determines differentiation to these phenotypes and whether pathogens provoke alternate programs. We find that, depending on the size of initial dose, *Listeria* infection drives CD4⁺ T cells to act as T_H or induces rapid polyclonal conversion to immunosuppressive T_{reg}. Conversion to T_{reg} depends on the TLR9 and IL-12 pathways elicited by CD8a⁺ dendritic cell (DC) sensing of danger-associated neutrophil self-DNA. These findings resolve long-standing questions regarding the conditional requirement for T_H amongst pathogens and reveal a remarkable degree of plasticity in the function of CD4⁺ T cells, which can be quickly converted to T_{reg} *in vivo* by infection-mediated immune modulation.

This is an open access article under the CC BY-NC-ND license (<http://creativecommons.org/licenses/by-nc-nd/4.0/>).

*Correspondence: jdolina@lji.org (J.S.D.), sps@lji.org (S.P.S.).

AUTHOR CONTRIBUTIONS

Research Conceptualization, J.S.D. and S.P.S.; Designed Experiments, J.S.D., L.L., N.B., M.J.P., and S.P.S.; Performed the Research, J.S.D., J.L., and R.Q.G.; RNA-Seq Processing, S.K. and J.A.G.; Analyzed Data, J.S.D., M.C., and S.P.S.; Statistical Analysis, J.S.D., S.K., and J.A.G.; Writing, J.S.D., M.C., and S.P.S.

DECLARATION OF INTERESTS

The authors declare no competing interests.

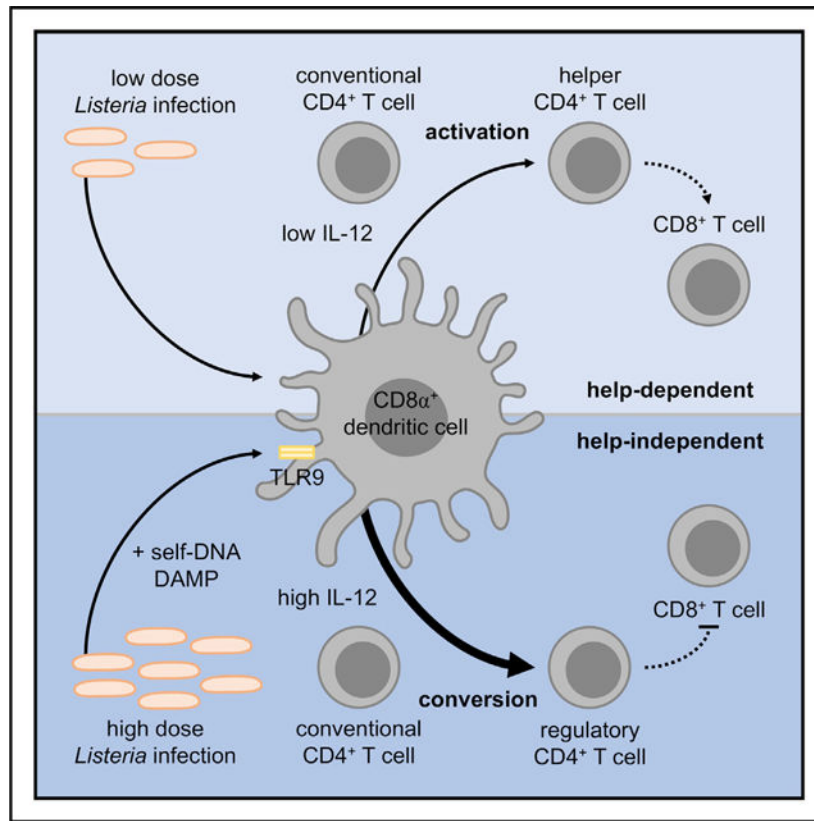
SUPPLEMENTAL INFORMATION

Supplemental Information can be found online at <https://doi.org/10.1016/j.celrep.2020.01.040>.

In Brief

Dolina et al. show that *Listeria* infectious dose drives conventional CD4⁺ T cells to act as T_H or mediates conversion to T_{reg}. Differentiation to T_{reg} dominates heightened doses and is promoted by CD8 α ⁺ DC TLR9 engagement of neutrophil self-DNA and IL-12 production, revealing plasticity in the function of CD4⁺ T cells.

Graphical Abstract



INTRODUCTION

CD4⁺ T cells comprise a broad array of phenotypic and functional lymphocyte subsets that assume specialized roles in the generation, differentiation, maintenance, and termination of immune responses (Yamane and Paul, 2013; Zhu et al., 2010). These include T-helper 1 (T_H1) cells that produce interferon- γ (IFN- γ) and are involved in responses to intracellular pathogens; T_H2 cells that produce interleukin-4 (IL-4), IL-5, and IL-13 for the control of helminth infections; and T_H17 cells that produce IL-17A/F in response to extracellular pathogens. The T_H1 subset in particular plays a crucial role in the priming and functional development of CD8⁺ T cell responses through the activation of antigen-presenting cells (APCs) via CD40L (Castellino and Germain, 2006; Haring et al., 2006; Janssen et al., 2003; Khanolkar et al., 2007; Schoenberger et al., 1998; Wiesel and Oxenius, 2012). A long-standing paradox in this regard concerns the conditional requirement for CD4⁺ T cell help by CD8⁺ T cell responses, with some immunogens needing CD4⁺ T cells to generate

effective primary and secondary CD8⁺ T cell responses, while others appear to do so in the absence of CD4⁺ T cells. Further complicating matters, the same immunogen has been reported to elicit both helper-dependent and helper-independent cytotoxic T lymphocyte (CTL) responses in different studies (Wiesel and Oxenius, 2012). Mechanisms underlying these distinct findings are poorly understood and likely reflect critical differences between experimental systems. Examples of such disparities may include direct activation of APCs or CD8⁺ T cells by pattern recognition receptors (PRRs) such as the prototypical Toll-like receptor (TLR) system (O'Neill et al., 2013) or various inflammatory cytokines involving type I IFN, IL-2, and IL-6 (Haring et al., 2006; Wiesel and Oxenius, 2012).

In addition to a helper role, CD4⁺ T cells also inhibit CD8⁺ T cells through their regulatory T cell (T_{reg}) subset, which relies on the expression of the transcription factor (TF) FoxP3 for its development, maintenance, and immunosuppressive function (Hori et al., 2003). T_{reg} are comprised of more stable naturally occurring T_{reg} (nT_{reg}), which develop in the thymus, and a peripheral T_{reg} (pT_{reg}) subset generated from FoxP3⁻ conventional CD4⁺ T cell precursors (Josefowicz et al., 2012). Both subsets have been implicated in mediating potent immunosuppression to a range of physiologic challenges, including microbial infection, atopy, and cancer, in which their absence leads to lethal autoimmunity in both mice and humans (Vignali et al., 2008). Whereas it is generally accepted that nT_{reg} become committed to a regulatory fate while still in the thymus (Josefowicz et al., 2012), the pathway(s) through which pT_{reg} are generated from conventional CD4⁺ T cells is less clear, with studies showing that this can occur through stimulation by a number of specific factors, including IL-10 (Bergmann et al., 2007), transforming growth factor b1 (TGF-b1) (Chen et al., 2003), low dose antigen (Kretschmer et al., 2005; Turner et al., 2009), and certain dendritic cell (DC) subsets (Tarbell et al., 2004; Yamazaki et al., 2007, 2008). The stability of pT_{reg} is also a matter of debate (Sakaguchi et al., 2013)—some studies have shown that loss of FoxP3 can allow development to T_H subsets (Williams and Rudensky, 2007), while others using alternative lineage-tracking methods argue that such reprogramming does not take place (Miyao et al., 2012).

These observations raise the possibility that pT_{reg} define a functionally discrete state that is achievable by naive CD4⁺ precursors, rather than a specific irreversible cellular fate, as it does for thymically derived nT_{reg}. Such a view immediately raises questions regarding the factors governing their generation *in vivo* by physiological conditions—which cell types or states can acquire T_{reg} function and how? The same questions are relevant for T_H1 cells that provide help for CD8⁺ T cell responses in light of their variable requirement among different infection models and the demonstration that infection can both stimulate and suppress the immune system (Bach, 2005; Rowe et al., 2012). Given that both subsets can develop from naive cells, we sought to evaluate the quantitative and kinetic parameters that govern the generation of T_H1 versus T_{reg} in the context of a pathogenic infection for which a variable dependence on CD4⁺ T cells has been reported.

RESULTS

Dose-Dependent Priming of CD4⁺ and CD8⁺ T Cell Subsets by *Listeria*

The CD8⁺ T cell response to the infectious pathogen *Listeria monocytogenes* (*Lm*) mirrors the variability reported for many infection models in that depending on the strain, inoculum dosage, route of delivery, and method of CD4⁺ T cell removal or blockade, these can be shown to be either dependent on or independent of CD4⁺ T cells (Bevan, 2004; Castellino and Germain, 2006; Khanolkar et al., 2007). We therefore sought to limit the variables to a single parameter—initial infectious dose. We evaluated the kinetics and magnitude of total and Ova_{257–264} antigen-specific (Ova-specific) CD8⁺ T cells, conventional (NK1.1⁻) CD4⁺ T cells, and regulatory (CD25⁺FoxP3⁺) CD4⁺ T cells (T_{reg}) at various time points following intravenous (i.v.) inoculation of C57BL/6 mice with low dose (LD; 1 × 10³ colony-forming units [CFUs]) or high-dose (HD; 1 × 10⁶ CFUs) *Lm actA*-Ova. Whereas both LD and HD infection produced CD8⁺ T cell responses that peaked at day 7 post-infection, the larger HD inoculum induced both Ova-specific and polyclonal CD8⁺ T cell responses of 3-fold greater magnitude (Figure 1A, upper panels). Both the conventional CD4⁺ T cell and T_{reg} response to HD infection displayed a biphasic pattern (Figure 1A, lower panels), with distinct peaks at days 1 and 7 noticeable for both subsets. Furthermore, the frequency of T_{reg} and fold change in the FoxP3⁺:FoxP3⁻ ratio within the total CD4⁺ T cell fraction was noticeably increased at day 1 after HD infection, whereas T_{reg} were decreased by day 7 due to the large expansion of conventional CD4⁺ T cells at later time points (Figures 1B and 1C).

We next determined the requirement of CD4⁺ T cells in CD8⁺ T cell generation as a function of initial pathogen dose. Depletion of CD4⁺ T cells prior to LD infection produced a characteristically smaller primary CD8⁺ T cell response consistent with a helper function for CD4⁺ T cells. Interestingly, CD4⁺ T cell depletion in the setting of HD infection led to a significantly greater primary CD8⁺ T cell response, as measured by both the number of Ova-specific cells and IFN-γ⁺ effectors (Figure 1D), and correlated with an increased T_{reg} frequency observed with HD infection at day 1 (Figures 1B and 1C). CD4⁺ T cells therefore restricted the primary expansion of antigen-specific CD8⁺ T cells responding to a larger infectious dose of *Lm*.

T_{reg} Restrict Primary CD8⁺ T Cell Responses to Higher Bacterial Burden and Impede Host Survival

Given that T_{reg} can impact the development of a number of pathogen-driven responses (Belkaid and Tarbell, 2009; Mills, 2004) and the presence of elevated T_{reg} numbers within 1 day of HD infection, we tested whether FoxP3-expressing T_{reg} could limit the magnitude of the primary CD8⁺ T cell response. For this we used *Foxp3^{DTR-EGFP}* mice, which allow for the selective depletion of this subset by administration of diphtheria toxin (DT) (Figure S1A). This treatment did not affect the number of activated CD8⁺ T cells based on effector cytokine production as well as CD44, CD62L, and CD69 expression within 3 days after initial injection (the time at which animals in this study were infected) (Figures S1B–S1E) (Kim et al., 2007). T_{reg} removal in the setting of HD infection mirrored the effect of acute CD4⁺ T cell depletion in C57BL/6 mice, in which the primary CD8⁺ T cell response was of significantly increased magnitude as measured by Ova_{257–264}/H-2K^b-tetramer binding

and IFN- γ production. Superimposing CD4⁺ T cell depletion onto T_{reg} depletion yielded no additional effects (Figure 1E). These findings suggest that the absence of T_{reg} accounts for the effect of acute CD4⁺ T cell depletion and that T_{reg}, but not helper, activity is dominant in the CD4⁺ T cell response observed during HD infection.

In the setting of LD infection, removal of T_{reg} also resulted in a significantly greater Ova-specific CD8⁺ T cell number, indicating that T_{reg} restrain the generation of primary CD8⁺ T cell responses under these conditions (Figure 1E, left panel). As also reported in the *Lm* model (Pace et al., 2012), the population of Ova-specific CD8⁺ T cells primed in the absence of T_{reg} after LD infection were of lower functional avidity, as evidenced by the unchanged absolute number of CD8⁺ T cells producing IFN- γ in response to the Ova₂₅₇₋₂₆₄ peptide (Figure 1E, right panel) and reduced affinity to the Ova₂₅₇₋₂₆₄/H-2K^b-tetramer (Figure 1F). Depletion of CD4⁺ T cells in DT-treated *Foxp3^{DTR-EGFP}* mice led to a significant reduction in both Ova-specific and IFN- γ ⁺ CTLs, showing that conventional FoxP3⁻CD4⁺ T cells were still required to maximize the primary CD8⁺ T cell response after LD infection. These data indicate that although T_{reg} restrict the primary expansion of CD8⁺ T cells and influence their functional avidity, the LD response is still substantively dependent on CD4⁺ T cells, presumably through their actions as T_H.

Various genetic deletions of pathways involved in innate and/or adaptive arms of the immune system have demonstrated equal significance for host survival against wild-type (WT) *Lm* strains (Ishii et al., 2005; Pamer, 2004). To determine whether the presence of T_{reg} was indeed limiting for resistance against WT *Lm*, survival was assessed in C57BL/6 versus *Foxp3^{DTR-EGFP}* mice. Whereas many mice succumbed to infection after lethal challenge with WT *Lm* Ova when T_{reg} were left intact, depletion of T_{reg} resulted in 100% survival (Figure 1G). Therefore, T_{reg} limit CD8⁺ T cell responses during exposure to elevated *Lm* infectious doses that is important for host resistance.

T_{reg} Suppress Primary Responses to *Listeria* with a Distinct Kinetic Compared to T_H

To further understand when T_{reg} were important, delayed CD4⁺ T cell depletion following HD infection established that suppression of the antigen-specific CD8⁺ T cell response was extant within 3 to 4 days after initial infection (Figures 2A and 2B). Specific blockade of the CD40-CD40L pathway 1 day before but not 3 days after LD infection resulted in reduced Ova-specific CD8⁺ T cell responses, consistent with the key role of this pathway in early APC activation. In contrast, CD40-CD40L blockade in the setting of HD infection did not increase the CD8⁺ T cell response as observed when CD4⁺ T cells were depleted (Figure 2C). These results demonstrate a clear difference in the role of CD4⁺ T cells in the priming of CD8⁺ T cells that is only revealed by varying the initial inoculum dose: CD4⁺ T cells function as conventional T_H to activate or license APCs within the initial 2 days of the LD response (Janssen et al., 2003; Schoenberger et al., 1998), but assume a persistent regulatory function to restrict expansion after HD infection with a different kinetic from that of T_H.

In contrast to the effect seen in the setting of LD infection, CD40-CD40L blockade did not significantly reduce the magnitude of the CD8⁺ T cell response in HD infected animals regardless of T_{reg} depletion (Figure 2D). This further suggested that only HD infection induced a *bona fide* T_H-independent response in the presence or absence of T_{reg}.

This appeared to depend on the greater inflammatory capacity of the quantitatively larger initial dose rather than the increased antigen it contains, as supplementing LD infection with additional cell-associated antigen in a non-inflammatory context (*Act-mOva H-2kb^{-/-}* splenocyte immunization) did not overcome the requirement for T_H (Figures S2A and S2B). Taken together, our findings demonstrate that the degree of inflammation associated with the initial infectious dose of *Lm* determines the requirement for CD4⁺ T cells in the priming of antigen-specific CD8⁺ T cells and can discriminate their roles as T_H versus T_{reg}.

Acute Infection Induces Rapid Polyclonal Conversion of Conventional CD4⁺ Cells to T_{reg}

The demonstration that CD4⁺ T_{reg} actively limit the response magnitude of primary *Lm*-specific CD8⁺ T cells (Figure 1E), together with the significant increase in the T_{reg} numbers within 1 day of HD infection (Figure 1A), prompted us to investigate factors responsible for their generation at this early time point. We analyzed correlates of polyclonal T cell activation using the *Nr4a1^{GFP}* (Nur77-GFP) mouse, which reports on T cell receptor (TCR)-mediated signaling but not inflammatory stimuli (Moran et al., 2011) in conjunction with induction of the acute activation marker CD69 in conventional CD4⁺ T cell and FoxP3⁺ T_{reg} populations as well as in total CD8⁺ T cells (Figure 3A). Consistent with previous findings, T_{reg} from naive animals displayed a 2-fold higher level of Nur77-GFP reporter expression compared to conventional CD4⁺ T cells, reflecting the fact that T_{reg} receive stronger TCR signals due to constant engagement of self-antigens in the periphery (Moran et al., 2011). Although each T cell subset displayed a distinct background level of GFP expression, only HD infection resulted in a significantly increased GFP signal across each cell type. Similarly, HD infection resulted in strong polyclonal induction of CD69 expression in all T cell subsets.

This raised the possibility that the rapid increase in FoxP3⁺ T_{reg} observed 1 day after HD infection was the product of conversion from conventional CD4⁺ precursors. To address this, we performed adoptive transfer of polyclonal conventional (non-EGFP-expressing) CD4⁺ T cells from CD45.1⁺ *Foxp3^{EGFP}* mice to CD45.2⁺ mice, which were subsequently infected with LD or HD *Lm actA-Ova*. This system allowed visualization of the conversion from conventional EGFP⁻ CD4⁺ T cells to EGFP⁺ CD4⁺ T_{reg} *in vivo*. When the recipients were analyzed 1 day after infection, a substantial fraction of the transferred conventional CD4⁺ T cells from mice given HD but not LD infection were found to have undergone conversion to phenotypic T_{reg} (FoxP3⁺), as judged by expression of EGFP (Figure 3B) and FoxP3 (Figures S3A and S3B). The newly converted FoxP3⁺CD4⁺ T cells also showed enhanced proliferative potential, as indicated by increased Ki-67 expression (Figure S3C). In further support of these observations, we found that endogenous CD45.2⁺ conventional CD4⁺ T cells in recipient animals displayed increased FoxP3 and CD25 expression following HD infection (Figure S3D). Newly converted FoxP3⁺CD4⁺ T cells could no longer be detected in the spleens of infected animals by day 7, indicating that rapid conversion is either an unstable phenotype or unidirectional terminal differentiation event. Rapid conversion also occurred after dose titration of non-attenuated WT *Lm Ova* using the adoptive transfer system described above (Figures 3C and S3E). These data collectively demonstrate that rapid polyclonal conversion of conventional CD4⁺ T cells to FoxP3⁺ T_{reg} occurs in a dose-dependent manner following infection with both attenuated and WT *Lm* strains.

We next determined whether the newly converted CD25⁺ FoxP3⁺ cells were capable of functionally suppressing CD8⁺ T cell responses *in vitro* and *in vivo*. To test for *in vitro* suppression, CD45.1⁺CD4⁺FoxP3⁺ (EGFP⁺) T cells were re-isolated following *in vivo* conversion and used in a suppression assay for the inhibition of CD3/CD28-driven proliferation of polyclonal CD8⁺ responder T cells (T_{resp}). Converted CD45.1⁺CD4⁺FoxP3⁺ T cells significantly suppressed CD8⁺ T_{resp} proliferation, while CD45.1⁺FoxP3⁻ (EGFP⁻) conventional CD4⁺ T cells that originated from the same transferred population but that had not undergone conversion were not suppressive (Figure 4A). Two distinct approaches were next taken for assessing the *in vivo* suppressive capacity of T_{reg} that arise through conversion. The first involved selective removal of stable T_{reg} but not those induced through conversion. To achieve this, we modified the DT-mediated depletion of stable T_{reg} in *Foxp3^{DTR-EGFP}* mice by terminating DT treatment 1 day prior to HD infection in an effort to leave the converted CD4⁺ T cells intact as the sole source of T_{reg}. When the peak magnitude of antigen-specific CD8⁺ T cell responses measured in *Foxp3^{DTR-EGFP}* mice treated with DT throughout the experiment (days -3 to 5), affecting both pre-existing and converted T_{reg}, was compared to that observed in mice treated only prior to infection (days -3, -1), approximately half of the total T_{reg}-mediated suppression could be ascribed to the T_{reg} that arose through conversion, which are retained in this latter group (Figure 4B). We then performed a second set of experiments in which only converted T_{reg} would be available for suppressive function *in vivo*. This involved the transfer of non-DTR/EGFP-expressing conventional CD4⁺ T cells from CD45.1⁺ *Foxp3^{EGFP}* mice (Figure S3F) to *Foxp3^{DTR-EGFP}* mice treated throughout infection with DT. Under these circumstances, T_{reg} arising only through conversion (Figure S3G) displayed approximately half the total suppressive activity of the stable T_{reg} that were depleted by DT (Figure 4C). The inhibitory function of the converted T_{reg} was not only manifest on the reduced proliferative capacity of the antigen-specific CD8⁺ T cells but also on their capability to produce effector cytokines (Figure 4D). Taken together, these data demonstrate that the T_{reg} arising through conversion of polyclonal conventional CD4⁺ T cells possess potent suppressive activity *in vitro* and *in vivo*.

TLR9 Expression by CD8α⁺ DCs Sustains Production of IL-12 and T_{reg} Responses

We then sought to understand the mechanism by which HD infection limited the CD8⁺ T cell response and drove conventional CD4⁺ T cell conversion to T_{reg}. No perturbation in the primary CD8⁺ T cell response magnitude was seen after HD infection of *Tlr2^{-/-}* and *Tlr7^{-/-}* mice, two TLRs linked to *Lm*, as well as of *Tlr4^{-/-}* mice (irrelevant for Gram-positive bacteria). In contrast, *Tlr9^{M7Btlr}* mice (expressing a dysfunctional variant of TLR9 harboring an S359P amino acid substitution) displayed a marked increase in the absolute number of Ova-specific CD8⁺ T cells generated in the presence of CD4⁺ T cells (Figure 5A). CD4⁺ T cell depletion in *Tlr9^{M7Btlr}* animals revealed that TLR9 deficiency completely accounted for immunoregulation exerted by CD4⁺ T cells during HD infection (Figure 5B). In concordance, *Tlr9^{M7Btlr}* animals displayed increased numbers of CD4⁺ and CD8⁺ effectors but fewer T_{reg} compared to C57BL/6 mice (Figure S4A). These data show that TLR9 is a critical PRR that limits acute activation of CD8⁺ T cells during HD infection.

To explore the mechanistic link between TLR9 signaling and inflammation-associated suppression of CD8⁺ T cells, we examined an array of cytokines and chemokines produced

within 6 h of HD infection in C57BL/6 and *Tlr9^{M7Btlr}* mice. *Tlr9^{M7Btlr}* mice did not display any apparent defect in serum CXCL1 (KC) or CXCL2 (MIP-2), suggesting that neutrophil egress from bone marrow was upstream of and not related to TLR9. We also noted a subtle spike in serum IFN- γ but consistently decreased CCL2 (MCP-1), CXCL9 (MIG), CXCL10 (IP-10), and IL-12 (p70) in *Tlr9^{M7Btlr}* mice, suggesting a mixed phenotype, including an increased type II IFN response in the midst of defective leukocyte recruitment and polarization of T_H1 cells (Figures 5C and 5D). The serum proteome readout was then compared with upstream regulators (functional predictions) that actuate differential gene expression profiles of total splenic T_{reg} sorted as EGFP⁺ from *Foxp3^{EGFP}* mice after 24 h of exposure to HD *Lm actA-Ova*. Of the top 50 significant upstream regulators predicted to give rise to the *Lm*-generated T_{reg} signature, commonalities were found to exist between the causal IFN- α , IFN- β , IFN- γ , and IL-12 (p70) gene network and serum data (Figures 5E and S4B). Kinetic analysis of these cytokines over 24 h revealed a severe defect in the ability of *Tlr9^{M7Btlr}* mice to produce IL-12 (p70). The small difference in IFN- γ observed previously at 6 h appeared trivial as inflammation increased from 12 to 24 h, and no strain-specific differences were observed in type I IFN production (Figure 5F).

These data suggested that a link existed between IL-12 (p70) production and the conversion of conventional CD4⁺ cells to T_{reg}. To further elucidate this, transcriptional analysis was performed among sorted FoxP3-EGFP⁻ conventional CD4⁺ T cells and FoxP3-EGFP⁺ T_{reg} 24 h after LD or HD infection. Genes differentially expressed relative to the naive state were subjected to Gene Ontology (GO) pathway analysis (Figure S5A). Gene sets from GO pathways having *Z* scores > 1.5 were further characterized by differential expression analysis (Figure S5B). Although LD infection did not reveal global changes in cell function, HD infection showed enrichment for pathways related to activation, proliferation, and survival in both conventional and T_{reg} CD4⁺ subsets. Conventional CD4⁺ T cells sorted as EGFP⁻ exhibited a transcriptional profile favoring the development of T_{reg} (*Ifng*, *Stat1*, *Tnfrsf9*, *Stat3*, *Bcl6*, *Icos*, and *Card11*), suggesting that some of these cells were activated and capable of transitioning to a state supportive of FoxP3 upregulation. Moreover, the FoxP3-EGFP⁺ T_{reg} clearly initiated a T_H1 differentiation program (*Tbx21*, *Il12rb1*, *Il12rb2*, *Irf1*, *Irf8*, *Stat1*, *Socs3*, and *Relb*), despite expressing FoxP3. Together, these *in silico* findings support the conversion of conventional CD4⁺ T cells to a T_{reg} differentiation program and indicate that a cell type similar to T_H1-like T_{reg} expressing *Tbx21* (T-bet) contributes to the early accumulation of CD25⁺FoxP3⁺ T_{reg} during HD *Lm* infection. T-bet expression within FoxP3⁺ T_{reg} is thought to enable focused counter-regulation within a heterogeneous T_{reg} cell population during infection (Levine et al., 2017), but these T_H1-like T_{reg} are inherently limited to an incomplete T_H1 differentiation due to lack of *Il12rb2* expression (Koch et al., 2012). Our data support instead a scenario in which excess IL-12 (p70) exposure driven by TLR9 signaling contributes to transient FoxP3 upregulation in a fully differentiated T_H1 cell expressing *Tbx21* and *Il12rb2* at day 1 following HD *Lm* infection, leading to acquisition of suppressor function.

The cellular source of TLR9 and IL-12 (p70) was next investigated. A significant transient increase in *Tlr9* mRNA was seen at day 1 in whole spleens isolated from HD-infected C57BL/6 mice (Figure 6A) and was largely limited to CD11c⁺ cells (Figure 6B). TLR9 is known to signal through IFN regulatory factor 7 (IRF7) for type I IFN induction and a

separate nuclear factor κ B (NF- κ B) axis relevant for pro-inflammatory cytokine production (O'Neill et al., 2013). Given that multiple NF- κ B DNA-binding sites exist within the *III2a* and *III2b* gene loci (Figures S6A–S6C), we assessed which cells were actively translocating cytoplasmic NF- κ B to the nucleus using p65-GFP knockin mice in which GFP is fused to the N terminus of the p65 subunit of canonical NF- κ B. We noted that universal transcription of p65-GFP increased in multiple splenic DC and macrophage (Mac) subtypes in these animals after 24 h of HD infection but not in B cells (Figure 6C). Visualization of the subcellular localization of p65-GFP showed that CD8 α^+ DCs exclusively translocated p65-GFP inside nuclei relative to TLR9^{lo-hi} expression and infection. Plasmacytoid DCs (pDCs) also mobilized p65-GFP to the nucleus, but this did not correlate with intracellular TLR9 expression (Figure 6D). In addition, CD8 α^+ DC populations isolated from HD-infected C57BL/6 mice primarily produced IL-12 (p40) by flow cytometric analysis, and this was decreased in *Tlr9^{M7Blr}* mice (Figure 6E).

To further study the role of the CD8 α^+ DC subset in T_{reg} conversion, we used BATF3 (basic leucine zipper TF, activating transcription factor [ATF]-like 3)-deficient mice, which have restricted the development of CD103⁺ and CD8 α^+ DC populations (Belz and Nutt, 2012). Naive and HD-infected *Batf3^{-/-}* mice were comparable in having reduced absolute numbers and frequencies of TLR9⁺CD8 α^+ DCs (Figures S7A–S7C), and importantly, *Batf3^{-/-}* mice did not display an increased FoxP3⁺:FoxP3⁻ ratio compared to the rapid enrichment of T_{reg} consistently observed in C57BL/6 mice after 24 h of HD infection (Figure 6F). In summary, these data collectively support that TLR9 expression by CD8 α^+ DC controls IL-12 (p70) production proportional to the initial *Lm* infectious dose, and this is directly or indirectly linked to the conversion of conventional CD4⁺ T cells into FoxP3-expressing T_{reg}.

IL-12 Triggering by Sequence-Specific CpG Oligodeoxynucleotides Drives Suppression and Enhances FoxP3 Expression

TLR9 is an endosomal PRR capable of recognizing naturally derived cytosine-phosphate-guanine (CpG) oligodeoxynucleotides (ODNs) in a 2:2 stoichiometry (Ohto et al., 2015). CpG ODNs contain unmethylated CpG dinucleotides in particular sequence contexts (CpG motifs) present at a 20-fold excess in bacterial genomes and in the 16.6-kb mitochondrial genome, which is essentially of prokaryotic origin (Ries et al., 2013). Eukaryote genomes have otherwise co-evolved to hypermethylate and decrease CpG motif frequency (Krieg et al., 1995) to potentially endow TLR9 with the ability to recognize these motifs as both pathogen- and danger-associated molecular patterns (PAMP and DAMP, respectively). As synthetic CpG ODN type A (CpG-A) is known to stimulate IFN- α release, whereas type B (CpG-B) leads to the production of IL-12 (Heit et al., 2004; Krug et al., 2001), we performed a functional comparison of these ODNs to further our conclusions. We confirmed the latter differential effect on IL-12 (p70) in the absence of infection compared to CpG controls (containing swapped GpC motifs) (Figure S8A). Most important, we found that CpG-B but not CpG-A rapidly increased the frequency of T_{reg} *in vivo* (Figure 7A). To extend this, CpG-A and CpG-B injections were superimposed on LD infection to determine the effect on the antigen-specific CD8⁺ T cell response. CpG-B alone suppressed the primary response of splenic Ova-specific CD8⁺ T cells in C57BL/6 mice. Moreover, this suppression by CpG-B was mediated by T_{reg}, as the absence of these cells in DT-treated

Foxp3^{DTR-EGFP} mice negated this effect (Figure 7B). Furthermore, CpG-B was no longer immunosuppressive when IL-12 (p70) was blocked during LD *Lm* infection (Figure 7C). These data show that direct TLR9 recognition of CpG ODN is linked to rapid IL-12 (p70)-driven T_{reg} expansion and immunosuppression.

Lastly, we sought the source of DNA to trigger this TLR9-driven pathway. We hypothesized that *Lm*-derived DNA was irrelevant because direct engulfment of phagosome-restricted listeriolysin O-deficient *Lm* (*Lm* *DLLO*) by activated WT and TLR9-deficient Macs has been shown to lead to robust type I IFN production *in vitro* (Herskovits et al., 2007). In search of a naturally produced TLR9 ligand, host mitochondrial DNA (mtDNA) and nuclear DNA (nDNA) in addition to *Lm* DNA itself were measured in cell-free/RNA-free serum samples of mice 0–48 h after HD infection. Circulating mtDNA (*12s* and *Trlev*) was detected at a log higher concentration compared to nDNA (*Neb* and *Becn1*) and at 2 logs greater than *Lm* DNA (*Ova*, *mpl*, and *plcB*), with a notable spike occurring at 4 h post-infection (Figure 7D). Release of mtDNA at 4 h into the sera of infected animals did not appear to be related to hepatocyte damage beginning at 6 h post-infection (Figure 7E). Serum mtDNA rather appeared to have arisen from an early 2–4 h neutrophil response shown by depletion of these cells with an anti-Ly6G monoclonal antibody (Figure 7F).

The relevance of extracellular self-DNA to the observed inhibition of the CD8⁺ T cell response was next examined by several strategies. First, we found that the immunosuppression of CD8⁺ T cell responses to HD infection of C57BL/6 hosts was alleviated by DNase I treatment, but this treatment did not increase the magnitude of the CD8⁺ T cell response beyond that produced by T_{reg} deletion in DT-treated *Foxp3^{DTR-EGFP}* mice (Figure 7G). Prior work has shown that self-DNA expelled by neutrophils in the form of neutrophil extracellular traps (NETs) is a critical defense mechanism for the rapid clearance of *Lm*. Disruption of NET integrity via DNase I treatment before and continuously throughout infection was similarly demonstrated to negatively affect the survival of lethally challenged hosts (Chen et al., 2017; Witter et al., 2016). By delaying initiation of DNase I treatment until 1.5 h post-infection to leave the early neutrophil NET response intact, we found that DNase I-treated mice displayed a distinct survival advantage against primary WT *Lm* *Ova* infection (Figure 7H). Extracellular self-DNA thus likely acts as a double-edged sword that is critical for defense against *Lm*, as it is essential for NET integrity, but whose presence leads to TLR9 activation and the subsequent rapid generation of T_{reg} through conversion.

Taken together, these results support the notion that self-DNA endogenously released following HD infection mirrors the effects of synthetic CpG-B, in which heightened IL-12 (p70) endows T_{reg} conversion and immunosuppression. The upregulation of FoxP3 in conventional CD4⁺ T cells has been reported to occur as early as 2–3 days after a combination of TCR, IL-2, and TGF-β1 stimulation *in vitro* (Pillai et al., 2007; Walker et al., 2003). We questioned whether IL-12 (p70) could enhance FoxP3 expression in this context within 1 day. To address this, conventional CD4⁺ T cells were sorted as EGFP⁻ from *Foxp3^{EGFP}* mice and subjected to CD3/CD28 cross-linking *in vitro*. We found that a 24-h TGF-β1 treatment induced ~20%–40% FoxP3 expression in FoxP3-EGFP⁻ conventional CD4⁺ T cells. The addition of IL-12 (p70) to TGF-β1-containing cultures pushed FoxP3

expression to ~50%–60% positivity, whereas IL-12 (p70) addition alone did not support a T_{reg} program. FoxP3 expression seemed to divert into FoxP3^{lo} and FoxP3^{hi} patterns, with IL-12 (p70) primarily enhancing FoxP3^{lo} frequency. Importantly, IL-12 (p70) did not augment FoxP3 expression if cells lacked IL-12Rb2 (Figures 7I and 7J). Exogenous IL-2 addition to the cultures was not necessary, but rather was provided by the conventional CD4⁺ T cells in autocrine (data not shown). FoxP3-EGFP⁻ conventional CD4⁺ T cells sorted from CD45.1⁺ *Il12rb2*^{-/-} *Foxp3*^{EGFP} mice similarly displayed reduced expression of FoxP3 compared to WT cells *in vivo* after transfer to and HD infection of C57BL/6 hosts (Figure S8B). In summation, this report shows that the innate immune system translates perceived danger in the form of self-DNA into IL-12 (p70)-based inflammation, directly contributing to conventional CD4⁺ T cell conversion to T_{reg} in reshaping cell-mediated adaptive immunity.

DISCUSSION

This study initially sought to resolve the confusing and often-contradictory literature surrounding the role of CD4⁺ T cells in the generation of CD8⁺ T cell responses through analysis of an immunogen for which the T cell help requirement has been reported to vary. Our results provide substantial insights in this regard by showing that, depending on the initial infectious dose of a pathogen, CD4⁺ T cells assume distinct roles as either T_H or T_{reg} . At low infectious dose, CD4⁺ T cells function as classical helpers for the CD8⁺ T cell response through CD40L-dependent APC activation, whereas infection with higher doses of the same pathogen causes rapid conversion of polyclonal conventional CD4⁺ T cells to a functional regulatory state in which both pathogen-specific and total CD8⁺ T cell responses are suppressed. These rapidly converted T_{reg} are distinct from both p T_{reg} and stable n T_{reg} in many key features, including *in vitro* suppressive potential on a per-cell basis, which appears to be lower than both of the other T_{reg} subsets (Fantini et al., 2007; Fu et al., 2004; Wang et al., 2007), and in their functional persistence, which appears to be limited to 3 or 4 days following generation of these cells. Our findings reveal a hitherto unappreciated rapid sensory plasticity in the immune response that can both quantify a given pathogenic threat and, depending on its magnitude, either direct CD4⁺ T cells to enhance the generation of CD8⁺ effectors to control the infection or quickly mount a significant regulatory response through rapid conversion to protect the host from the pathologic effects of systemic inflammation. It is notable that in the latter case, the duration of the regulatory event is nonetheless sufficiently brief to enable the former to occur. These findings shed light on the position occupied by CD4⁺ T cells in the regulation and functional specialization of adaptive immune responses and on their capacity to integrate the activities of the innate and adaptive arms of the immune response.

The generation of T_{reg} via conversion of conventional naive CD4⁺ T cells has been suggested by a variety of mechanisms, including a study showing that bystander systemic inflammation induced by polyI:C could generate p T_{reg} capable of suppressing CD4⁺ T cell responses within 7 days *in vivo* or 5 days *in vitro* if TGF- β 1 was also provided exogenously (Thompson et al., 2016). The present study demonstrates that conversion of conventional CD4⁺ T cells can occur within 24 h of exposure to an infectious pathogen *in vivo* in a dose-dependent manner or *in vitro* via a combination of IL-12 (p70) and TGF- β 1

exposure. The difference in conversion time may involve TGF- β 1 availability and relative potency of stimulating a single TLR pathway by polyI:C (TLR3) causing a gradual rise in type I IFN, versus CpG motif-specific (TLR9) stimulation of IL-12 (p70) production shown herein to rapidly fluctuate. The common mechanistic link between type I IFN and IL-12 (p70) signaling within a T cell is that both cytokines induce phosphorylation of signal transducer and activator of transcription 1 (pSTAT1) heterodimerization (Gollob et al., 1998; Jacobson et al., 1995; Szabo et al., 1995). Similarly, induction of pSTAT1 homodimerization after conventional T cell exposure to IFN- γ caused a rapid 24-h increase in FoxP3 expression with accompanied *in vitro* and *in vivo* suppressive capacity (Wang et al., 2006). It is notable that STAT1-deficient mice develop more severe experimental autoimmune encephalomyelitis due to lack of a suppressor population (presumably nT_{reg}) in the CD25⁺CD4⁺ compartment (Nishibori et al., 2004). Although eventual induction of pSTAT1 leads to the upregulation of SMAD7 (refers to homologies to *Caenorhabditis elegans Sma* and *Drosophila Mad* gene families) in feedforward inhibition of TGF- β 1-induced pSMAD3 binding to conserved non-coding DNA sequence 1 (CNS1) in the *Foxp3* promoter, pSTAT1 DNA-binding sites have been found in the proximal *Foxp3* promoter supportive of transcription (Kleiter et al., 2010; Ouaked et al., 2009; Zheng et al., 2010).

Transdifferentiation of T_{reg} to other functional states has also been demonstrated, with lineage-marked exT_{reg} capable of assuming T_H1 or T_H17 functional phenotypes, for example (Bailey-Bucktrout et al., 2013; Miyao et al., 2012). Our study is distinct, however, in reporting such a sizeable polyclonal population of CD4⁺ T cells differentiating from naive CD4⁺ T cells to FoxP3-expressing T_{reg} with *in vivo* suppressor function as an immediate consequence of systemically produced IL-12 (p70). The dynamics of this process in terms of both the generation and persistence of these cells as mentioned above is notable, with our phenotypic analysis, adoptive transfer, and depletion studies demonstrating that although the converted T_{reg} and their suppressive effects arise quickly following HD infection, both disappear within 3–4 days, essentially coincident with the full primary expansion of the effector CD8⁺ T cells needed to contain the progressive infection (Mielke et al., 1988). Perhaps differences in this regard exist in the kinetics in which opposing SMAD7 and pSTAT1 influence *Foxp3* transcription and acquisition of suppressor function.

Our results clearly demonstrate that converted T_{reg} are not only numerically significant but also, as a population, are endowed with considerable *in vivo* suppressor capacity, with two distinct assays showing these cells to be roughly equipotent to the stable T_{reg} that exist in the host prior to infection. We also found that the T_{reg} arising through rapid conversion are able to restrict both pathogen-specific CD8⁺ T cell responses and the cytokine-mediated expansion of polyclonal memory phenotype CD4⁺ and CD8⁺ T cells (data not shown) that have long been observed to follow infection or exposure to bacterial components (Tough et al., 2000). As such bystander activation of memory T cells has been implicated in autoimmune conditions such as diabetes and multiple sclerosis, the regulation in the context of infection is crucial (Pane and Coulson, 2015; Pender and Burrows, 2014). The risk posed by unrestrained self-reactive memory T cells would seem to represent a suitable rationale for the response to acute inflammation revealed by our study in which a substantial population of polyclonal naive CD4⁺ T cells are rapidly pressed into service as regulators.

As mentioned above, however, these suppressor cells have a brief lifespan and disappear just as primed pathogen-specific CD8⁺ T cells needed to control infection expand.

FoxP3 is a lineage-defining marker for T_{reg} whose expression is dictated by complex upstream gene expression events shaped by TCR, IL-2, and TGF-β signaling (Gavin et al., 2007; Hill et al., 2007). Although Nur77 induction data suggest that both conventional CD4⁺ T cells and T_{reg} receive early TCR stimulation, it is difficult to envision from both a numerical and kinetic basis that the large population of FoxP3-expressing T_{reg} derived through conversion is *Lm* specific, and it is furthermore unlikely that these converted cells are the previously described T_{H1}-like nT_{reg} (Koch et al., 2012) due to presence of both *Tbx21* and *Ill2rb2* transcripts in sorted FoxP3⁺ cells and responsiveness to IL-12 (p70). More recent studies suggest that self-reactive conventional FoxP3⁻CD4⁺ T cells escape thymic deletion and exist in steady-state tolerance in tissue niches alongside antigen-specific FoxP3⁺ nT_{reg} (Hogquist and Jameson, 2014). Non-deletional tolerance can be lost in the periphery upon exposure to self-antigens experimentally contained within *Lm* (Legoux et al., 2015). Thus, given that self-reactive conventional CD4⁺ T cells exist at low numbers during homeostasis and expand upon infection with *Lm*, we speculate that the excessive inflammation associated with HD infection generates a cytokine network including but not limited to IL-2, IL-12, and TGF-β1, thereby supporting rapid differentiation to FoxP3⁺ T_{reg}.

The splenic CD8α⁺DEC-205⁺ DC subset identified as a key APC for conversion in our study is capable of profound intrinsic TGF-β1 production and uniquely specialized to gradually convert conventional CD4⁺ T cells to pT_{reg} *in vivo* in the absence of inflammation. Additionally, TLR3 ligation inhibits TGF-β1 secretion and subsequent T_{reg} induction by this DC subtype, possibly linked to the slower kinetic of polyI:C-induced conversion (Yamazaki et al., 2008). In this work, we revealed that CD8α⁺ DCs are the relevant source of an IL-12 (p70)-driven T_{reg} response via DC TLR9 sensing of extracellular host mtDNA released by the neutrophil response to HD infection. The innate immune system has therefore likely evolved to interpret mtDNA-contained CpG ODNs as a DAMP to appropriately fine-tune downstream adaptive responses via T_{reg} to balance autoimmune reactions to self versus effective pathogen clearance. Complex sepsis syndrome in humans is characterized by a two-phase immune response, where initial hyperinflammation and septic shock are followed by a phase of immune paralysis associated with the incapacity to develop adaptive immunity against secondary infection or latent viral reactivation. Septic patients consistently display elevated serum mtDNA, which can be engulfed by CD11c⁺ APC and ligate TLR9 to suppress subsequent antigen-specific CD8⁺ T cell responses *in vivo* (Schäfer et al., 2016). The dosage of CpG ODNs is indeed critical in shaping CD4⁺ and CD8⁺ T cell proliferation, in which high doses constrain expansion and low doses promote or have no effect on T cell responses (Wingender et al., 2006).

The majority of circulating DNA found shortly after acute *Lm* infection is of mitochondrial and neutrophil origin. Neutrophils were first identified to release NETs comprised of nDNA, histones, and granules in a process associated with cell death (Brinkmann et al., 2004). Under certain conditions, neutrophils release NETs comprised of mtDNA within 15 min via hypopolarized mitochondrial movement to the plasma membrane followed by a later 36-h phase in which cells die with NET content becoming enriched in nDNA (Lood et al., 2016;

Yousefi et al., 2009). Regardless of the source, whether mtDNA is actively incorporated in NETs or passively released by dying neutrophils, we present evidence that CpG ODNs contained therein are immunomodulatory.

With respect to our original question regarding the conditional requirement of CD4⁺ T cell help for CD8⁺ T cells, it is worth noting that the antigen-specific CD8⁺ T cell response induced under conditions of acute inflammation (HD infection) is of a larger comparative magnitude in the absence of CD4⁺ T cells than that induced by LD infection and yet is still somewhat dependent on T cell help to achieve an optimal response magnitude. This is in contrast to the situation of CD8⁺ T cell responses in LD infection, which we show to be paradoxically constrained by stable T_{reg} yet nonetheless strongly dependent on T_H. Whether these differences are due to cytokine-mediated effects on proliferation or direct activation of APCs remains to be elucidated, but our findings highlight the intrinsic limitations in describing a given CD8⁺ T cell response as help dependent or independent based solely on response magnitude (Castellino and Germain, 2006; Haring et al., 2006; Khanolkar et al., 2007; Wiesel and Oxenius, 2012). Our findings reveal that T_H-independent CD8⁺ T cell responses are observed when immunogens induce excessive inflammation associated with the infectious dose amidst primary activation (Figures 1D, S2A, and S2B) or secondary challenge, although responses of optimal magnitude and memory functionality are induced when CD4⁺ T cells are present (data not shown). These observations help to resolve the often-contradictory literature with respect to the T_H dependence of CD8⁺ T cells by revealing that initial pathogen dose plays a large and durable role in the fate and function of the ensuing response. Finally, our findings are of particular relevance for understanding the immunobiology of infection, as well as for the efficacy of vaccine strategies that induce a strong inflammatory response. Elucidation of the cells and signaling pathways that guide rapid conversion of conventional CD4⁺ T cells to T_{reg} should allow the development of more effective approaches to immune regulation.

STAR★METHODS

Detailed methods are provided in the online version of this paper and include the following:

LEAD CONTACT AND MATERIALS AVAILABILITY

Further information and requests for resources and reagents should be directed to and will be fulfilled by the Lead Contact, Dr. Joseph S. Dolina (jdolina@lji.org). This study did not generate new unique reagents.

EXPERIMENTAL MODEL AND SUBJECT DETAILS

Animals—Male and female C57BL/6, *Batf3*^{-/-}, *Foxp3*^{EGFP} (FoxP3-EGFP), *Foxp3*^{DTR-EGFP}, *H-2kb*^{-/-}, *I112rb2*^{-/-}, *Tlr2*^{-/-}, *Tlr4*^{-/-}, *Tlr7*^{-/-}, and *Tlr9*^{M7Btlr} mice (The Jackson Laboratory, Bar Harbor, ME) were used in these experiments. *Foxp3*^{DTR-EGFP} mice contain an internal ribosome entry site (IRES), human diphtheria toxin receptor (DTR), and an enhanced green fluorescent protein (EGFP) downstream of the internal stop codon of the *Foxp3* locus (Kim et al., 2007). Mice expressing *Gallus gallus* ovalbumin under the *Actb* (b-actin) promoter (*Act*-mOva) were originally obtained from Marc K. Jenkins (University

of Minnesota, Minneapolis, MN) and crossed to *H-2kb^{-/-}* mice on the C57BL/6 background generating *Act-mOva H-2kb^{-/-}* mice as described previously (Feau et al., 2011; Janssen et al., 2005). *Nr4a1^{GFP}* (Nur77-GFP) reporter mice were generated as described (Moran et al., 2011) from the laboratory of Kristin A. Hogquist (University of Minnesota). Homozygous p65-GFP knockin mice acquired from Manolis Pasparakis (University of Cologne, Cologne, Germany) were engineered with GFP fused to the N terminus of the first exon of p65 to avoid interference with C-terminal DNA-binding and transactivating domains thereby preserving NF- κ B function (De Lorenzi et al., 2009). Animals used in experiments were 8–12 weeks of age and maintained/bred in the La Jolla Institute for Immunology vivarium under specific pathogen-free conditions in accordance with guidelines of the Association for Assessment and Accreditation of Laboratory Animal Care International.

Infections and immunizations—*Listeria monocytogenes* (*Lm*) derived from the wild-type (WT) 10403S background either deficient in the actin assembly-inducing protein alone (*Lm actA*) or expressing amino acids spanning 138–338 of full-length ovalbumin (WT *Lm Ova* and *Lm actA-Ova*) were obtained from the laboratory of Daniel A. Portnoy (University of California, Berkeley, CA). Bacteria were cultured in BBL brain heart infusion medium (Becton, Dickinson and Company, Sparks, MD) at 37°C, back-diluted to log-phase ($OD_{600} = 0.075\text{--}0.100$), washed, and re-suspended in 1:3 PBS.

Primary *in vivo* infections were conducted via intravenous (i.v.) injection of low dose (LD; 1×10^3 CFU) or high dose (HD; 1×10^6 CFU) *Lm DactA* or *Lm actA-Ova* in the caudal vein. For dual immunizations to *Lm*, 5×10^6 *Act-mOva H-2kb^{-/-}* splenocytes were delivered i.v. concurrent with primary infection as noted. WT *Lm Ova* infections were delivered i.v. over a $1 \times 10^3\text{--}1 \times 10^5$ CFU range for short-term *in vivo* visualization of conventional CD4⁺ T cell conversion to T_{reg} and a $1 \times 10^4\text{--}2.5 \times 10^4$ CFU range for extended survival experiments.

METHOD DETAILS

***In vivo* antibody and small molecule treatments**—The GK1.5 hybridoma (ATCC, Manassas, VA) and MR1 hybridoma originally produced by Alejandro Aruffo (Bristol-Myers Squibb Pharmaceutical Research Institute, Seattle, WA) (Noelle et al., 1992) were cultured in CELLline 1000 bioreactors (Wheaton, Millville, NJ) to obtain large quantities of anti-CD4 and anti-CD40L antibodies, respectively. Anti-Ly6G (1A8) and anti-IL-12 (p70) (R2–9A5) were otherwise externally purchased for experiments (BioXCell, West Lebanon, NH). For early CD4⁺ T cell depletion, anti-CD4 was delivered intraperitoneally (i.p.) in the following regimen: 200 μ g at day –5, 100 mg at day –2, and 100 μ g at day 5 relative to a day 0 infection. Animals that had CD4 T cells intact during initial infection still received 200 mg anti-CD4 at day 5. For delayed CD4⁺ T cell depletion, a single bolus of 400 μ g anti-CD4 was delivered at days 3, 4, or 5 i.p.. For early CD40L blockade, 150 μ g i.p. injections of anti-CD40L were given to animals at days –1 and 2. For delayed CD40L blockade, mice received a single 250 μ g i.p. injection of anti-CD40L at day 3 post-infection. Specific depletion of neutrophils was achieved via delivery of 500 μ g anti-Ly6G i.p. one day prior to infection.

CD25⁺FoxP3⁺CD4⁺ T_{reg} depletion was achieved in *Foxp3^{DTR-EGFP}* mice via i.p. administration of 100 µg/kg diphtheria toxin (DT) from *Corynebacterium diphtheriae* (Sigma-Aldrich, St. Louis, MO) separated into quadruplicate 25 µg/kg i.p. injections at days -3, -1, 2, and 5 relative to a day 0 infection. In some experiments timing of DT injection was limited to only days -3 and -1 to differentiate early versus late T_{reg} activity *in vivo*.

Agonistic 20-mer CpG oligodeoxynucleotides (ODN) were used to trigger supplementary TLR9 bystander inflammation *in vivo* as repeated 50 µg i.p. injections at days -1 and 0 in relation to LD *Lm actA-Ova* infection. ODN 1585 (CpG-A) 5'-ggGGTCAACGTT GAgggggg-3' and ODN 1668 (CpG-B) 5'-tccatgacgttcctgatgct-3' (underlined represents the RRCGY Y CpG motif with R as purine and Y as pyrimidine, upper case are phosphodiester bases, and lower case are phosphorothioate bases) were used in these studies (InvivoGen, San Diego, CA). Control ODN counterparts consisting of the same backbone containing GpC dinucleotide motifs were used as references. A mechanistic interrogation of a role for IL-12 in bystander inflammation-induced suppression was conducted with consecutive 300 mg anti-IL-12 (p70) i.p. co-injections alongside CpG-B delivery at days -1 and 0 in similar experiments.

TLR9 engagement of endogenous DNA present in the extracellular space of infected animals was conversely digested via repeat i.v. injections of 2000 U DNase I (Roche, Mannheim, Germany) at 1.5, 3, 6, and 24 h after infection. Animals infected with *Lm actA-Ova* in this context were used to measure the Ova-specific CD8⁺ T cell response magnitude at day 7 post-infection, described below. This brief exposure of DNase I was also used to evaluate long term survival of subjects lethally challenged with titrated doses of WT *Lm Ova*.

Alanine aminotransferase assay—Mice were sacrificed by lethal i.p. injection of 500 mg/kg ketamine HCl (Ketathesia; Henry Schein Animal Health, Dublin, OH) and bled via the retro-orbital venous plexus. Blood was collected in BD Microtainer SST tubes (BD Biosciences, Franklin Lakes, NJ) containing polymer gel and 100 U heparin (Fresenius Kabi USA, Schaumburg, IL) at 0, 2, 4, and 6 h post-infection. Sera samples were purified, and alanine aminotransferase (ALT) concentration was determined by mixing 20 µL serum with 200 µL liquid ALT working buffer (Pointe Scientific, Canton, MI). The reaction was incubated for 180 s at 37°C. Absorbance at 340 nm was read at 0, 60, 120, and 180 s time points with a kinetic read function using a SpectraMax M2 Microplate Reader equipped with SoftMax Pro (v5.3b12) software (Molecular Devices, San Jose, CA). OD₃₄₀/min was used to calculate ALT concentration.

Enzyme-linked immunosorbent assay (ELISA) and multiplex assay—Heparinized blood/serum was collected at 0, 6, 12, and 24 h post-infection as described above. Mouse IFN-α2/4 Platinum ELISA (eBioscience, San Diego, CA), mouse IFN-β VeriKine ELISA (PBL Assay Science, Piscataway, NJ), and mouse IL-12 (p70) as well as human/mouse TGF-β1 ELISA Ready-SET-Go (Invitrogen, Carlsbad, CA) kits were used in these studies according to the manufacturer's instructions. Absorbance was read at 450 nm using a SpectraMax M2 Microplate Reader equipped with SoftMax Pro (v5.3b12) software (Molecular Devices). Sera were also analyzed using a MILLIPLEX MAP 32-plex mouse

cytokine/chemokine panel (EMD Millipore, Billerica, MA) and analyzed on a Luminex MAGPIX System with xPONENT (v4.2) software (Luminex, Austin, TX).

Reverse-transcription/quantitative PCR (RT/Q-PCR)—Total RNA was isolated from whole spleen and cell sorted DC/T cell populations via the Trizol method (Invitrogen). Samples were reverse-transcribed using High Capacity RNA-to-cDNA Master Mix (Applied Biosystems, Foster City, CA). Q-PCR was performed using AB Fast SYBR Green Master Mix on an AB StepOne Plus Real-Time PCR System (Applied Biosystems). QuantiTect primers for *Mus musculus Tlr2*, *Tlr4*, *Tlr7*, and *Tlr9* (QIAGEN, Valencia, CA), and self-designed primers for *Mus musculus* hypoxanthine phosphoribosyltransferase 1 (*Hprt1*; Fwd, 5'-CTCCGCCGGCTTCCTCCTCA-3'; Rev, 5'-ACCTGGTTCATCATCGCTAATC-3') were used for detection.

Serum mitochondrial DNA (mtDNA), nuclear DNA (nDNA), and *Lm* DNA quantification—Cell-free serum was collected as described previously without use of heparin to avoid cellular lysis. RNA-free DNA was isolated using the column-based DNeasy Blood & Tissue kit coupled with 12 mAU proteinase K and 28 U RNase A exposure (QIAGEN), and DNA concentration was determined with high-sensitivity (>10 ng/mL) using the Qubit dsDNA HS Assay kit and Qubit Fluorometer (Invitrogen). All Q-PCR was performed using AB Fast SYBR Green Master Mix on an AB StepOne Plus Real-Time PCR System (Applied Biosystems). The Novagen NovaQUANT Mouse Mitochondrial to Nuclear Ratio kit was used to amplify both mtDNA (*12 s* and *Trlev*) and nDNA (*Neb* and *Becn1*) target genes in both samples and controls. Target DNA pre-amplification concentration was back-calculated based on 40 3 PCR cycles using titration curves generated from kit-provided WT DNA (LM) and ρ^0 DNA (LMBE4) (EMD Millipore).

In separate analyses, self-designed primers for ovalbumin model antigen (*Ova*; Fwd, 5'-GTCAGCAGAGGCTGGAGTGGA-3'; Rev, 5'-GGCGTTGGTTGCGATGTGCT-3') together with the *Lm* encoded zinc metalloproteinase (*mpI*; Fwd, 5'-CCAGTATTCGGCGG GATTGG-3'; Rev, 5'-GACCCACGCACACAGACATC-3') and broad-substrate range phospholipase C (*plcB*; Fwd, 5'-GCAACGGAA GACATGGTAGCAA-3'; Rev, 5'-GTAGTCCGCTTTTCGCCCTTT-3') were used to detect *Lm actA*-Ova-specific target concentration in sera. Purified reference RNA-free DNA was collected via the DNeasy Blood & Tissue kit (QIAGEN) from a *Lm actA*-Ova midiprep exposed to lysis buffer containing 0.5 mg/mL lysozyme (Thermo Scientific, Rochester, NY), 20 mM Tris-Cl, and 2 mM EDTA (TE) for 30 min at 37°C followed with 1.2% Triton X-100 TE treatment for 10 min at 25°C. *Lm* pre-amplification target concentration was back-calculated using *Lm* genomic titration curves.

Spleen mononuclear cell isolation—Spleens were excised from the abdominal cavities of naive and infected/immunized mice and homogenized through sterile 70 μ m cell strainers (Fisher Scientific, Pittsburgh, PA) in RPMI 1640 medium containing 10% fetal bovine serum. Viable mononuclear cells were quantified via Trypan Blue exclusion on a Vi-CELL XR cell viability analyzer (Beckman Coulter, Indianapolis, IN).

***In vivo* T_{reg} conversion and functional suppression**—Conventional CD4⁺ T cells were isolated from CD45.1⁺ *Foxp3*^{EGFP} or CD45.1⁺ *Il12rb2*^{-/-} *Foxp3*^{EGFP} mice using the EasySep Mouse CD4⁺ T Cell Isolation kit (STEMCELL Technologies Inc., Vancouver, BC, Canada) followed by fluorescent cell sorting and transfer of 3.5×10^6 EGFP⁻ T cells into C57BL/6 and *Foxp3*^{DTR-EGFP} mice. For conversion, separate groups of C57BL/6 mice were left naive or infected with LD or HD *Lm actA-Ova*. At days 1 and 7 post-infection, the percent of splenic CD45.1⁺FoxP3-EGFP⁻ cells that expressed EGFP, FoxP3, and Ki-67 was determined. For *in vivo* suppressor function of converted cells, day 7 CTL responses were analyzed in C57BL/6 and *Foxp3*^{DTR-EGFP} mice that had received a full day -3 to 5 DT regimen and 7.5×10^6 CD45.1⁺FoxP3-EGFP⁻ T cell transfer.

***In vitro* T cell suppressor assay**—Naive CD45.2⁺CD8⁺ T responder cells (T_{resp}) were negatively sorted using the EasySep Mouse CD8⁺ T Cell Isolation kit (STEMCELL Technologies Inc.) and stained with CellTrace Violet (CTV; Life Technologies, Carlsbad, CA). CD45.1⁺CD4⁺FoxP3-EGFP⁻ T cells that had experienced HD *Lm actA-Ova* infection for 24 h in C57BL/6 mice were re-isolated using the EasySep Mouse CD4⁺ T Cell Isolation kit (STEMCELL Technologies Inc.) followed by fluorescent cell sorting CD45.1⁺CD45.2⁻FoxP3-EGFP⁺ and CD45.1⁺CD45.2⁻FoxP3-EGFP⁻ cells. 2.5×10^4 CD45.2⁺CD8⁺ T_{resp} were placed in co-culture with graded numbers of sex-matched, magnetic/fluorescent cell sorted CD45.1⁺FoxP3-EGFP⁺ (T_{reg}) or EGFP⁻ (conventional) CD4⁺ T cells and 1.25 mL washed Mouse T-Activator anti-CD3/CD28 Dynabeads (GIBCO) in a 96-well round-bottom plate for 72 h. Cell proliferation of CD45.2⁺CD8⁺ T_{resp} was determined by flow cytometry based on dilution of CTV. Percent suppression was calculated as the percent difference in absolute number of dividing T_{resp} in wells containing EGFP⁺ or EGFP⁻ CD4⁺ T cells to the average absolute number of dividing T_{resp} in wells without addition of EGFP⁺ or EGFP⁻ CD4⁺ T cells. Replication index, representative of only T_{resp} that had responded to anti-CD3/CD28 stimulation, was also determined for the cultures.

***In vitro* simulation of T_{reg} conversion**—Conventional CD4⁺ T cells were isolated from CD45.1⁺ *Foxp3*^{EGFP} or CD45.1⁺ *Il12rb2*^{-/-} *Foxp3*^{EGFP} mice using the EasySep Mouse CD4⁺ T Cell Isolation kit (STEMCELL Technologies Inc.) followed by fluorescent cell sorting of EGFP⁻ T cells. 2.3×10^5 CD4⁺FoxP3-EGFP⁻ T cells were placed in culture with 5 μ L washed Mouse T-Activator anti-CD3/CD28 Dynabeads (GIBCO, Carlsbad, CA) and 1 μ g/mL anti-IL-4 (11B11) (BioLegend, San Diego, CA) in a 96-well round-bottom plate for 24 h. Select wells contained 5 ng/mL rmTGF- β 1 and 10 ng/mL rmIL-12 (p70) (R&D Systems, Minneapolis, MN). Nuclear FACS staining of EGFP, FoxP3, and T-bet were used to measure conventional CD4⁺ T cell conversion to phenotypic T_{reg}.

Flow cytometry and fluorescent cell sorting—Cells were stained with fluorochrome-tagged antibodies from BD Biosciences, BioLegend, eBioscience, PBL Assay Science, Rockland Immunochemicals (Limerick, PA), Thermo Scientific, and Tonbo Biosciences (San Diego, CA) (Table S1). Identification of cells in this study was achieved by a FSC-A versus SSC-A gate set at 30–250K versus 0–200K, respectively, including all leukocytes with the goal of excluding debris/reticulocytes/RBCs. Next, a singlet gate was set from 50–100K FSC-W parameter. A SSC-W singlet gate was not applied to avoid misconstruing

blasting T cells as doublets. In general, cell viability within this gate was >97% using Live/Dead Fixable Yellow Dead Cell Stain kit (Invitrogen). For most experiments, live/dead stains were not deemed necessary unless mRNA was analyzed which employed sorting out dead cells from analyzed populations. For T cells, a $\text{TCR}\beta^+\text{NK1.1}^-$ gate was applied to exclude $\text{NK1.1}^{\text{hi}}\text{TCR}\beta^-$ NK cells and $\text{NK1.1}^{\text{lo}}\text{TCR}\beta^{\text{lo-hi}}$ NKT cells. The resultant population contained 100% T cells, and further gates for CD4, CD8a, CD45.1, and CD45.2 were applied per the requirements of individual experiments. CD4^+ T cells were subsequently gated as conventional (FoxP3^-) versus T_{reg} ($\text{CD25}^+\text{FoxP3}^+$). $\text{H-2K}^{\text{b}}\text{-Ova}$ ($\text{Ova}_{257-264}$ bound to H-2K^{b}) iTA α tetramer (MBL International, Woburn, MA) was used to identify Ova-specific CD8^+ T cells. Any other analyte staining including but not limited to CD44, CD69, intracellular cytokine detection, and EGFP/GFP expression was based off FMO and isotype controls set at 0.5% positivity in negative control samples. FoxP3-EGFP expression within a transferred conventional CD4^+ T cell population in the presence of *Lm* infection was further defined based off uninfected controls. For APCs, a general MHC-II(I-A/I-E)^+ gate was first set. $\text{B220}^+\text{CD11c}^-$ B cells, $\text{B220}^+\text{CD11c}^+$ pDCs, and $\text{B220}^-\text{CD11c}^+$ macrophage (Mac) and DC populations could be readily identified downstream of this. The $\text{B220}^-\text{CD11c}^+$ bulk gate was further dissected via CD11b, $\text{CD11c}^{\text{lo-hi}}$, CD8a, CD103, and F4/80 expression for deeper identification of Mac and DC subsets. PBMC populations were analyzed for absence of $\text{CD4}^+\text{TCR}\beta^+$ cells during CD4^+ T cell depletion experiments, and lack of $\text{CD11b}^+\text{Ly6G}^{\text{hi}}$ cell presence was confirmed in neutrophil depletion experiments before proceeding.

Cell surface staining of 3.0×10^6 splenic mononuclear cells isolated directly *ex vivo* or various numbers of cells cultured *in vitro* was performed by specific antibody labeling for 15 min at 4°C in FACS Buffer (1:3 PBS containing 2% fetal bovine serum and 0.1% NaN_3). Cells were fixed in BD Cytofix/Cytoperm (BD Biosciences). Nuclear protein staining was achieved using the FoxP3 Staining Set (eBioscience). For intracellular T cell cytokine detection, cells were re-stimulated with 2 $\mu\text{g}/\text{mL}$ $\text{Ova}_{257-264}$ peptide (AnaSpec, Fremont, CA) for 5 h. Intracellular cytokine detection in APC populations was measured after 5 h of stimulation with 5 ng/mL phorbol 12-myristate 13-acetate (PMA) and 500 ng/mL ionomycin (Sigma-Aldrich). Both cytokine procedures featured concurrent blocking with 1 $\mu\text{L}/\text{mL}$ GolgiPlug and 1 $\mu\text{L}/\text{mL}$ GolgiStop during culture and permeabilization with BD Perm/Wash (BD Biosciences) after fixation.

Data were collected on a BD FACS Canto II (BD Immunocytometry Systems, San Jose, CA) and analyzed using FlowJo (v9.7.5 and v10.4.2) software (Tree Star Inc., Ashland, OR). Fluorescent cell sorting of CD45.1^+ , CD45.2^+ , FoxP3-EGFP^+ , and/or FoxP3-EGFP^- cells was performed using BD FACSAria I, BD FACSAria II, and BD FACSAria Fusion cell sorters (BD Immunocytometry Systems).

ImageStream— p65-GFP knockin mice were infected with HD *Lm actA-Ova* for 24 h and splenocytes were surface stained as in traditional flow cytometry for identification of APC subset expression of MHC-II(I-A/I-E) , B220, CD11b, CD11c, CD8a, CD103, and F4/80 followed by identification of intracellular targets including endosomal TLR9, cytoplasmic/nuclear GFP, and DNA using 4',6-diamidino-2-phenylindole (DAPI; Molecular Probes, Eugene, OR). Cells were collected using an Amnis ImageStream^X mk II imaging

flow cytometer with INSPIRE (v99.0.0.0) software and analyzed using IDEAS (v6.2.183.0) software (Amnis Inc., Seattle, WA). Briefly, a morphology mask of nuclei was defined with DAPI, which included all pixels within the outmost image contour. To quantify translocation of p65-GFP to the nuclei of cells, the similarity score within the DAPI-masked area was calculated as the log transformed Pearson's correlation coefficient for DAPI and GFP image components and reported as the Median Similarity Morphology of ~1000–6000 events/sample (μ_1 = TLR9^{lo-hi}; μ_2 = naive-24 h).

RNA sequencing (RNA-Seq)—Total RNA was purified using the Direct-zol RNA MiniPrep Plus and RNA Clean & Concentrator-25 kits (Zymo Research, Irvine, CA). RNA quality and quantity was assessed using an Agilent 2100 Bioanalyzer with a RNA 6000 Pico kit (Agilent Technologies, Santa Clara, CA) resulting in all samples producing RIN scores above 9.0. 5 ng of total RNA was then amplified using the Smart-seq2 pro- tocol (Picelli et al., 2014). A 1:1 ratio of Agencourt AMPure XP beads (Beckman Coulter) were used to purify resulting cDNA, and 1 ng cDNA was subsequently used to prepare a sequencing library with the Nextera XT DNA Library Prep kit (Illumina, San Diego, CA). Both whole-transcriptome amplification and sequencing library preparations were performed in a 96-well format to reduce assay-to-assay variability. Quality control steps were included to determine total RNA quality and quantity, the optimal number of PCR pre-amplification cycles, and fragment size selection. The resulting libraries were deep sequenced on the HiSeq 2500 System in Rapid Run mode (Illumina) using 50-bp single-end reads ($\sim 6.0 \times 10^6$ reads per condition).

Bioinformatics analysis of RNA-Seq—The single-end reads that passed Illumina filters were filtered for reads aligning to tRNA, rRNA, adaptor sequences, and spike-in controls. Reads were then aligned to UCSC mm10 reference genome using TopHat (v1.4.1) software (Trapnell et al., 2009). DUST scores were calculated with PRINSEQ Lite (v0.20.3) software (Schmieder and Edwards, 2011) and low-complexity reads (DUST > 4) were removed from the BAM files. Alignment results were parsed via the SAMtools (Li et al., 2009) to generate SAM files. Read counts to each genomic feature were obtained with Python HTSeq (v0.6.0) software (Anders et al., 2015) using the union option. After removing absent features (zero counts in all samples), raw counts were imported to R (v3.1.0) Bioconductor (v3.0) package DESeq2 (v1.6.3) (Love et al., 2014) to identify differentially expressed genes among samples. DESeq2 normalizes counts by dividing each column of the count table (samples) by the size factor of this column. The size factor is calculated by dividing the samples by geometric means of the genes bringing count values to a common scale suitable for comparison. p values for differential expression were calculated using binomial test for differences between the base means of two conditions. p values were then adjusted for multiple test correction using the Benjamini Hochberg algorithm (Benjamini and Hochberg, 1995) to control the false discovery rate. Genes were considered differentially expressed between two groups of samples when DESeq2 analysis resulted in an adjusted p value of <0.05.

Bio function analysis of gene-ontology (GO) term enrichment of pathways related to T cell activation, differentiation, proliferation, death/survival, and adhesion/movement

showing enrichment among genes differentially expressed (filtered on $p < 0.05$) as well as upstream regulator prediction of differentially expressed gene profiles compared among bulk endogenous FoxP3-EGFP⁺ T_{reg} fluorescently sorted from naive mice versus counterparts exposed to HD *Lm actA*-Ova for 24 h was conducted using Ingenuity Pathway Analysis (IPA; v01–07) software (QIAGEN).

p65 DNA binding site prediction—The consensus transcription factor DNA-binding preference of the highly conserved N-terminal Rel homology (RH) domain of p65 (RelA) was queried in the JASPAR database (Sandelin et al., 2004). Putative transcription factor binding sites were scanned for with the position-specific frequency matrix of p65 input over genomic DNA spanning 2 kb upstream and downstream of murine *I12a* and *I12b* loci with an >0.80 threshold.

QUANTIFICATION AND STATISTICAL ANALYSIS

Significant differences between experimental groups were calculated using the two-tailed Student's *t* test or one-way/two-way ANOVAs (with group comparisons $R \geq 3$) with multiple comparison Tukey's post *hoc* test or Dunnett's post *hoc* test relative to a control where appropriate. For survival curves, the Mantel-Cox and χ^2 tests were used to determine significance. Data analysis was performed using Prism (v7.0a and v8.0.2) software (GraphPad Software Inc., La Jolla, CA). Numbers in histograms and scatterplots represent percentage. All data in bar, scatter, and line graphs indicate means \pm SEM. Values of $p < 0.05$ were regarded as being statistically significant and noted as * < 0.05 , ** < 0.01 , *** < 0.001 , and **** < 0.0001 . † < 0.05 , †† < 0.01 , ††† < 0.001 , and †††† < 0.0001 notations were used with reports of ANOVA alongside multiple comparisons tests. Each experiment in this report was replicated 2 or 3 times to ensure reproducibility and reach statistical power of the results.

DATA AND CODE AVAILABILITY

These data presented in this manuscript are tabulated in the main paper and in the supplementary materials. RNA-seq metadata are archived in the NCBI gene expression omnibus (GEO) as series GSE106554.

Supplementary Material

Refer to Web version on PubMed Central for supplementary material.

ACKNOWLEDGMENTS

We thank C. Kim, K. Van Gunst, L. Nosworthy, D. Hinz, and R. Simmons at the La Jolla Institute for Immunology Imaging Facility for technical assistance with the fluorescence-activated cell sorting (FACS) experiments. Y. Altman at the Sanford Burnham Prebys Medical Discovery Institute Flow Cytometry Core helped conduct the ImageStream acquisition and analysis. NIH grant R01 AI107010 supported this publication (S.P.S.). NIH-funded equipment was supported by grants S10 RR027366 and S10 OD016262 and included BD FACSAria II cell sorters and the Illumina HiSeq 2500 System, respectively.

REFERENCES

- Anders S, Pyl PT, and Huber W (2015). HTSeq—a Python framework to work with high-throughput sequencing data. *Bioinformatics* 31, 166–169. [PubMed: 25260700]
- Bach J-F (2005). Infections and autoimmune diseases. *J. Autoimmun.* 25 (Suppl), 74–80. [PubMed: 16278064]
- Bailey-Bucktrout SL, Martinez-Llordella M, Zhou X, Anthony B, Rosenthal W, Luche H, Fehling HJ, and Bluestone JA (2013). Self-antigen-driven activation induces instability of regulatory T cells during an inflammatory autoimmune response. *Immunity* 39, 949–962. [PubMed: 24238343]
- Belkaid Y, and Tarbell K (2009). Regulatory T cells in the control of host-microorganism interactions (*). *Annu. Rev. Immunol.* 27, 551–589. [PubMed: 19302048]
- Belz GT, and Nutt SL (2012). Transcriptional programming of the dendritic cell network. *Nat. Rev. Immunol.* 12, 101–113. [PubMed: 22273772]
- Benjamini Y, and Hochberg Y (1995). Controlling the False Discovery Rate: A Practical and Powerful Approach to Multiple Testing. *J. R. Stat. Soc. Ser. A Stat. Soc.* 57, 289–300.
- Bergmann C, Strauss L, Zeidler R, Lang S, and Whiteside TL (2007). Expansion and characteristics of human T regulatory type 1 cells in co-cultures simulating tumor microenvironment. *Cancer Immunol. Immunother.* 56, 1429–1442. [PubMed: 17265021]
- Bevan MJ (2004). Helping the CD8(+) T-cell response. *Nat. Rev. Immunol.* 4, 595–602. [PubMed: 15286726]
- Brinkmann V, Reichard U, Goosmann C, Fauler B, Uhlemann Y, Weiss DS, Weinrauch Y, and Zychlinsky A (2004). Neutrophil extracellular traps kill bacteria. *Science* 303, 1532–1535. [PubMed: 15001782]
- Castellino F, and Germain RN (2006). Cooperation between CD4+ and CD8+ T cells: when, where, and how. *Annu. Rev. Immunol.* 24, 519–540. [PubMed: 16551258]
- Chen W, Jin W, Hardegen N, Lei K-J, Li L, Marinos N, McGrady G, and Wahl SM (2003). Conversion of peripheral CD4+CD25- naive T cells to CD4+CD25+ regulatory T cells by TGF- β induction of transcription factor Foxp3. *J. Exp. Med.* 198, 1875–1886. [PubMed: 14676299]
- Chen S-T, Li F-J, Hsu T-Y, Liang S-M, Yeh Y-C, Liao W-Y, Chou T-Y, Chen N-J, Hsiao M, Yang W-B, and Hsieh SL (2017). CLEC5A is a critical receptor in innate immunity against *Listeria* infection. *Nat. Commun.* 8, 299. [PubMed: 28824166]
- De Lorenzi R, Gareus R, Fengler S, and Pasparakis M (2009). GFP-p65 knock-in mice as a tool to study NF- κ B dynamics in vivo. *Genesis* 47, 323–329. [PubMed: 19263497]
- Fantini MC, Dominitzki S, Rizzo A, Neurath MF, and Becker C (2007). In vitro generation of CD4+ CD25+ regulatory cells from murine naive T cells. *Nat. Protoc.* 2, 1789–1794. [PubMed: 17641646]
- Feau S, Arens R, Togher S, and Schoenberger SP (2011). Autocrine IL-2 is required for secondary population expansion of CD8(+) memory T cells. *Nat. Immunol.* 12, 908–913. [PubMed: 21804558]
- Fu S, Zhang N, Yopp AC, Chen D, Mao M, Chen D, Zhang H, Ding Y, and Bromberg JS (2004). TGF-beta induces Foxp3 + T-regulatory cells from CD4 + CD25 - precursors. *Am. J. Transplant.* 4, 1614–1627. [PubMed: 15367216]
- Gavin MA, Rasmussen JP, Fontenot JD, Vasta V, Manganiello VC, Beavo JA, and Rudensky AY (2007). Foxp3-dependent programme of regulatory T-cell differentiation. *Nature* 445, 771–775. [PubMed: 17220874]
- Gollob JA, Murphy EA, Mahajan S, Schnipper CP, Ritz J, and Frank DA (1998). Altered interleukin-12 responsiveness in Th1 and Th2 cells is associated with the differential activation of STAT5 and STAT1. *Blood* 91, 1341–1354. [PubMed: 9454765]
- Haring JS, Badovinac VP, and Harty JT (2006). Inflaming the CD8+ T cell response. *Immunity* 25, 19–29. [PubMed: 16860754]
- Heit A, Huster KM, Schmitz F, Schiemann M, Busch DH, and Wagner H (2004). CpG-DNA aided cross-priming by cross-presenting B cells. *J. Immunol.* 172, 1501–1507. [PubMed: 14734727]

- Herskovits AA, Auerbuch V, and Portnoy DA (2007). Bacterial ligands generated in a phagosome are targets of the cytosolic innate immune system. *PLoS Pathog.* 3, e51. [PubMed: 17397264]
- Hill JA, Feuerer M, Tash K, Haxhinasto S, Perez J, Melamed R, Mathis D, and Benoist C (2007). Foxp3 transcription-factor-dependent and -independent regulation of the regulatory T cell transcriptional signature. *Immunity* 27, 786–800. [PubMed: 18024188]
- Hogquist KA, and Jameson SC (2014). The self-obsession of T cells: how TCR signaling thresholds affect fate ‘decisions’ and effector function. *Nat. Immunol.* 15, 815–823. [PubMed: 25137456]
- Hori S, Nomura T, and Sakaguchi S (2003). Control of regulatory T cell development by the transcription factor Foxp3. *Science* 299, 1057–1061. [PubMed: 12522256]
- Ishii KJ, Ito S, Tamura T, Hemmi H, Conover J, Ozato K, Akira S, and Klinman DM (2005). CpG-activated Thy1.2+ dendritic cells protect against lethal *Listeria monocytogenes* infection. *Eur. J. Immunol.* 35, 2397–2405. [PubMed: 16047338]
- Jacobson NG, Szabo SJ, Weber-Nordt RM, Zhong Z, Schreiber RD, Darnell JE Jr., and Murphy KM (1995). Interleukin 12 signaling in T helper type 1 (Th1) cells involves tyrosine phosphorylation of signal transducer and activator of transcription (Stat)3 and Stat4. *J. Exp. Med.* 181, 1755–1762. [PubMed: 7722452]
- Janssen EM, Lemmens EE, Wolfe T, Christen U, von Herrath MG, and Schoenberger SP (2003). CD4+ T cells are required for secondary expansion and memory in CD8+ T lymphocytes. *Nature* 421, 852–856. [PubMed: 12594515]
- Janssen EM, Droin NM, Lemmens EE, Pinkoski MJ, Bensinger SJ, Ehst BD, Griffith TS, Green DR, and Schoenberger SP (2005). CD4+ T-cell help controls CD8+ T-cell memory via TRAIL-mediated activation- induced cell death. *Nature* 434, 88–93. [PubMed: 15744305]
- Josefowicz SZ, Lu L-F, and Rudensky AY (2012). Regulatory T cells: mechanisms of differentiation and function. *Annu. Rev. Immunol.* 30, 531–564. [PubMed: 22224781]
- Khanolkar A, Badovinac VP, and Harty JT (2007). CD8 T cell memory development: CD4 T cell help is appreciated. *Immunol. Res.* 39, 94–104. [PubMed: 17917058]
- Kim JM, Rasmussen JP, and Rudensky AY (2007). Regulatory T cells prevent catastrophic autoimmunity throughout the lifespan of mice. *Nat. Immunol.* 8, 191–197. [PubMed: 17136045]
- Kleiter I, Song J, Lukas D, Hasan M, Neumann B, Croxford AL, Pedré X, Hövelmeyer N, Yoge N, Mildner A, et al. (2010). Smad7 in T cells drives T helper 1 responses in multiple sclerosis and experimental autoimmune encephalomyelitis. *Brain* 133, 1067–1081. [PubMed: 20354004]
- Koch MA, Thomas KR, Perdue NR, Smigielski KS, Srivastava S, and Campbell DJ (2012). T-bet(+) Treg cells undergo abortive Th1 cell differentiation due to impaired expression of IL-12 receptor b2. *Immunity* 37, 501–510. [PubMed: 22960221]
- Kretschmer K, Apostolou I, Hawiger D, Khazaie K, Nussenzweig MC, and von Boehmer H (2005). Inducing and expanding regulatory T cell populations by foreign antigen. *Nat. Immunol.* 6, 1219–1227. [PubMed: 16244650]
- Krieg AM, Yi AK, Matson S, Waldschmidt TJ, Bishop GA, Teasdale R, Koretzky GA, and Klinman DM (1995). CpG motifs in bacterial DNA trigger direct B-cell activation. *Nature* 374, 546–549. [PubMed: 7700380]
- Krug A, Rothenfusser S, Hornung V, Jahrsdörfer B, Blackwell S, Ballas ZK, Endres S, Krieg AM, and Hartmann G (2001). Identification of CpG oligonucleotide sequences with high induction of IFN- α / β in plasmacytoid dendritic cells. *Eur. J. Immunol.* 31, 2154–2163. [PubMed: 11449369]
- Legoux FP, Lim J-B, Cauley AW, Dikiy S, Ertelt J, Mariani TJ, Sparwasser T, Way SS, and Moon JJ (2015). CD4+ T Cell Tolerance to Tissue-Restricted Self Antigens Is Mediated by Antigen-Specific Regulatory T Cells Rather Than Deletion. *Immunity* 43, 896–908. [PubMed: 26572061]
- Levine AG, Medoza A, Hemmers S, Moltedo B, Niec RE, Schizas M, Hoyos BE, Putintseva EV, Chaudhry A, Dikiy S, et al. (2017). Stability and function of regulatory T cells expressing the transcription factor T-bet. *Nature* 546, 421–425. [PubMed: 28607488]
- Li H, Handsaker B, Wysoker A, Fennell T, Ruan J, Homer N, Marth G, Abecasis G, and Durbin R; 1000 Genome Project Data Processing Subgroup (2009). The Sequence Alignment/Map format and SAMtools. *Bioinformatics* 25, 2078–2079. [PubMed: 19505943]

- Lood C, Blanco LP, Purmalek MM, Carmona-Rivera C, De Ravin SS, Smith CK, Malech HL, Ledbetter JA, Elkon KB, and Kaplan MJ (2016). Neutrophil extracellular traps enriched in oxidized mitochondrial DNA are interferogenic and contribute to lupus-like disease. *Nat. Med.* 22, 146–153. [PubMed: 26779811]
- Love MI, Huber W, and Anders S (2014). Moderated estimation of fold change and dispersion for RNA-seq data with DESeq2. *Genome Biol.* 15, 550. [PubMed: 25516281]
- Mielke ME, Ehlers S, and Hahn H (1988). T-cell subsets in delayed-type hypersensitivity, protection, and granuloma formation in primary and secondary *Listeria* infection in mice: superior role of Lyt-2+ cells in acquired immunity. *Infect. Immun.* 56, 1920–1925. [PubMed: 2969373]
- Mills KHG (2004). Regulatory T cells: friend or foe in immunity to infection? *Nat. Rev. Immunol.* 4, 841–855. [PubMed: 15516964]
- Miyao T, Floess S, Setoguchi R, Luche H, Fehling HJ, Waldmann H, Huehn J, and Hori S (2012). Plasticity of Foxp3(+) T cells reflects promiscuous Foxp3 expression in conventional T cells but not reprogramming of regulatory T cells. *Immunity* 36, 262–275. [PubMed: 22326580]
- Moran AE, Holzappel KL, Xing Y, Cunningham NR, Maltzman JS, Punt J, and Hogquist KA (2011). T cell receptor signal strength in Treg and iNKT cell development demonstrated by a novel fluorescent reporter mouse. *J. Exp. Med.* 208, 1279–1289. [PubMed: 21606508]
- Nishibori T, Tanabe Y, Su L, and David M (2004). Impaired development of CD4+ CD25+ regulatory T cells in the absence of STAT1: increased susceptibility to autoimmune disease. *J. Exp. Med.* 199, 25–34. [PubMed: 14699080]
- Noelle RJ, Roy M, Shepherd DM, Stamenkovic I, Ledbetter JA, and Aruffo A (1992). A 39-kDa protein on activated helper T cells binds CD40 and transduces the signal for cognate activation of B cells. *Proc. Natl. Acad. Sci. USA* 89, 6550–6554. [PubMed: 1378631]
- O’Neill LAJ, Golenbock D, and Bowie AG (2013). The history of Toll-like receptors - redefining innate immunity. *Nat. Rev. Immunol.* 13, 453–460. [PubMed: 23681101]
- Ohto U, Shibata T, Tanji H, Ishida H, Krayukhina E, Uchiyama S, Miyake K, and Shimizu T (2015). Structural basis of CpG and inhibitory DNA recognition by Toll-like receptor 9. *Nature* 520, 702–705. [PubMed: 25686612]
- Ouaked N, Mantel P-Y, Bassin C, Burgler S, Siegmund K, Akdis CA, and Schmidt-Weber CB (2009). Regulation of the foxp3 gene by the Th1 cytokines: the role of IL-27-induced STAT1. *J. Immunol.* 182, 1041–1049. [PubMed: 19124747]
- Pace L, Tempez A, Arnold-Schrauf C, Lemaitre F, Bouso P, Fetler L, Sparwasser T, and Amigorena S (2012). Regulatory T cells increase the avidity of primary CD8+ T cell responses and promote memory. *Science* 338, 532–536. [PubMed: 23112334]
- Pamer EG (2004). Immune responses to *Listeria monocytogenes*. *Nat. Rev. Immunol.* 4, 812–823. [PubMed: 15459672]
- Pane JA, and Coulson BS (2015). Lessons from the mouse: potential contribution of bystander lymphocyte activation by viruses to human type 1 diabetes. *Diabetologia* 58, 1149–1159. [PubMed: 25794781]
- Pender MP, and Burrows SR (2014). Epstein-Barr virus and multiple sclerosis: potential opportunities for immunotherapy. *Clin. Transl. Immunology* 3, e27.
- Picelli S, Faridani OR, Björklund AK, Winberg G, Sagasser S, and Sandberg R (2014). Full-length RNA-seq from single cells using Smart-seq2. *Nat. Protoc.* 9, 171–181. [PubMed: 24385147]
- Pillai V, Ortega SB, Wang CK, and Karandikar NJ (2007). Transient regulatory T-cells: a state attained by all activated human T-cells. *Clin. Immunol.* 123, 18–29. [PubMed: 17185041]
- Ries M, Schuster P, Thomann S, Donhauser N, Vollmer J, and Schmidt B (2013). Identification of novel oligonucleotides from mitochondrial DNA that spontaneously induce plasmacytoid dendritic cell activation. *J. Leukoc. Biol.* 94, 123–135. [PubMed: 23610148]
- Rowe JH, Ertelt JM, and Way SS (2012). Foxp3(+) regulatory T cells, immune stimulation and host defence against infection. *Immunology* 136, 1–10. [PubMed: 22211994]
- Sakaguchi S, Vignali DAA, Rudensky AY, Niec RE, and Waldmann H (2013). The plasticity and stability of regulatory T cells. *Nat. Rev. Immunol.* 13, 461–467. [PubMed: 23681097]

- Sandelin A, Alkema W, Engström P, Wasserman WW, and Lenhard B (2004). JASPAR: an open-access database for eukaryotic transcription factor binding profiles. *Nucleic Acids Res.* 32, D91–D94. [PubMed: 14681366]
- Schäfer ST, Franken L, Adamzik M, Schumak B, Scherag A, Engler A, Schönborn N, Walden J, Koch S, Baba HA, et al. (2016). Mitochondrial DNA: An Endogenous Trigger for Immune Paralysis. *Anesthesiology* 124, 923–933. [PubMed: 26808636]
- Schmieder R, and Edwards R (2011). Quality control and preprocessing of metagenomic datasets. *Bioinformatics* 27, 863–864. [PubMed: 21278185]
- Schoenberger SP, Toes RE, van der Voort EI, Offringa R, and Melief CJ (1998). T-cell help for cytotoxic T lymphocytes is mediated by CD40-CD40L interactions. *Nature* 393, 480–483. [PubMed: 9624005]
- Szabo SJ, Jacobson NG, Dighe AS, Gubler U, and Murphy KM (1995). Developmental commitment to the Th2 lineage by extinction of IL-12 signaling. *Immunity* 2, 665–675. [PubMed: 7796298]
- Tarbell KV, Yamazaki S, Olson K, Toy P, and Steinman RM (2004). CD25+ CD4+ T cells, expanded with dendritic cells presenting a single auto-antigenic peptide, suppress autoimmune diabetes. *J. Exp. Med.* 199, 1467–1477. [PubMed: 15184500]
- Thompson LJ, Lai J-F, Valladao AC, Thelen TD, Urry ZL, and Ziegler SF (2016). Conditioning of naive CD4(+) T cells for enhanced peripheral Foxp3 induction by nonspecific bystander inflammation. *Nat. Immunol.* 17, 297–303. [PubMed: 26752376]
- Tough DF, Sun S, Zhang X, and Sprent J (2000). Stimulation of memory T cells by cytokines. *Vaccine* 18, 1642–1648. [PubMed: 10689142]
- Trapnell C, Pachter L, and Salzberg SL (2009). TopHat: discovering splice junctions with RNA-Seq. *Bioinformatics* 25, 1105–1111. [PubMed: 19289445]
- Turner MS, Kane LP, and Morel PA (2009). Dominant role of antigen dose in CD4+Foxp3+ regulatory T cell induction and expansion. *J. Immunol.* 183, 4895–4903. [PubMed: 19801514]
- Vignali DAA, Collison LW, and Workman CJ (2008). How regulatory T cells work. *Nat. Rev. Immunol.* 8, 523–532. [PubMed: 18566595]
- Walker MR, Kaspirowicz DJ, Gersuk VH, Bènard A, Van Landeghen M, Buckner JH, and Ziegler SF (2003). Induction of FoxP3 and acquisition of T regulatory activity by stimulated human CD4+CD25- T cells. *J. Clin. Invest.* 112, 1437–1443. [PubMed: 14597769]
- Wang Z, Hong J, Sun W, Xu G, Li N, Chen X, Liu A, Xu L, Sun B, and Zhang JZ (2006). Role of IFN-gamma in induction of Foxp3 and conversion of CD4+ CD25- T cells to CD4+ Tregs. *J. Clin. Invest.* 116, 2434–2441. [PubMed: 16906223]
- Wang J, Ioan-Facsinay A, van der Voort EIH, Huizinga TWJ, and Toes REM (2007). Transient expression of FOXP3 in human activated nonregulatory CD4+ T cells. *Eur. J. Immunol.* 37, 129–138. [PubMed: 17154262]
- Wiesel M, and Oxenius A (2012). From crucial to negligible: functional CD8+ T-cell responses and their dependence on CD4+ T-cell help. *Eur. J. Immunol.* 42, 1080–1088. [PubMed: 22539281]
- Williams LM, and Rudensky AY (2007). Maintenance of the Foxp3-dependent developmental program in mature regulatory T cells requires continued expression of Foxp3. *Nat. Immunol.* 8, 277–284. [PubMed: 17220892]
- Wingender G, Garbi N, Schumak B, Jüngerkes F, Endl E, von Bubnoff D, Steitz J, Striegler J, Moldenhauer G, Tüting T, et al. (2006). Systemic application of CpG-rich DNA suppresses adaptive T cell immunity via induction of IDO. *Eur. J. Immunol.* 36, 12–20. [PubMed: 16323249]
- Witter AR, Okunnu BM, and Berg RE (2016). The Essential Role of Neutrophils during Infection with the Intracellular Bacterial Pathogen *Listeria monocytogenes*. *J. Immunol.* 197, 1557–1565. [PubMed: 27543669]
- Yamane H, and Paul WE (2013). Early signaling events that underlie fate decisions of naive CD4(+) T cells toward distinct T-helper cell subsets. *Immunol. Rev.* 252, 12–23. [PubMed: 23405892]
- Yamazaki S, Bonito AJ, Spisek R, Dhodapkar M, Inaba K, and Steinman RM (2007). Dendritic cells are specialized accessory cells along with TGF- β for the differentiation of Foxp3+ CD4+ regulatory T cells from peripheral Foxp3 precursors. *Blood* 110, 4293–4302. [PubMed: 17699744]

- Yamazaki S, Dudziak D, Heidkamp GF, Fiorese C, Bonito AJ, Inaba K, Nussenzweig MC, and Steinman RM (2008). CD8+ CD205+ splenic dendritic cells are specialized to induce Foxp3+ regulatory T cells. *J. Immunol.* 181, 6923–6933. [PubMed: 18981112]
- Yousefi S, Mihalache C, Kozłowski E, Schmid I, and Simon HU (2009). Viable neutrophils release mitochondrial DNA to form neutrophil extracellular traps. *Cell Death Differ.* 16, 1438–1444. [PubMed: 19609275]
- Zheng Y, Josefowicz S, Chaudhry A, Peng XP, Forbush K, and Rudensky AY (2010). Role of conserved non-coding DNA elements in the Foxp3 gene in regulatory T-cell fate. *Nature* 463, 808–812. [PubMed: 20072126]
- Zhu J, Yamane H, and Paul WE (2010). Differentiation of effector CD4 T cell populations (*). *Annu. Rev. Immunol.* 28, 445–489. [PubMed: 20192806]

Highlights

- Low dose *Listeria* infection is help dependent and high dose is help independent
- High dose drives conventional CD4⁺ T cell conversion to immunosuppressive T_{reg}
- Conversion to T_{reg} depends on TLR9-mediated IL-12 production by CD8a⁺ DC
- TLR9 ligation of neutrophil self-DNA underlies the T_{reg} response to DAMP

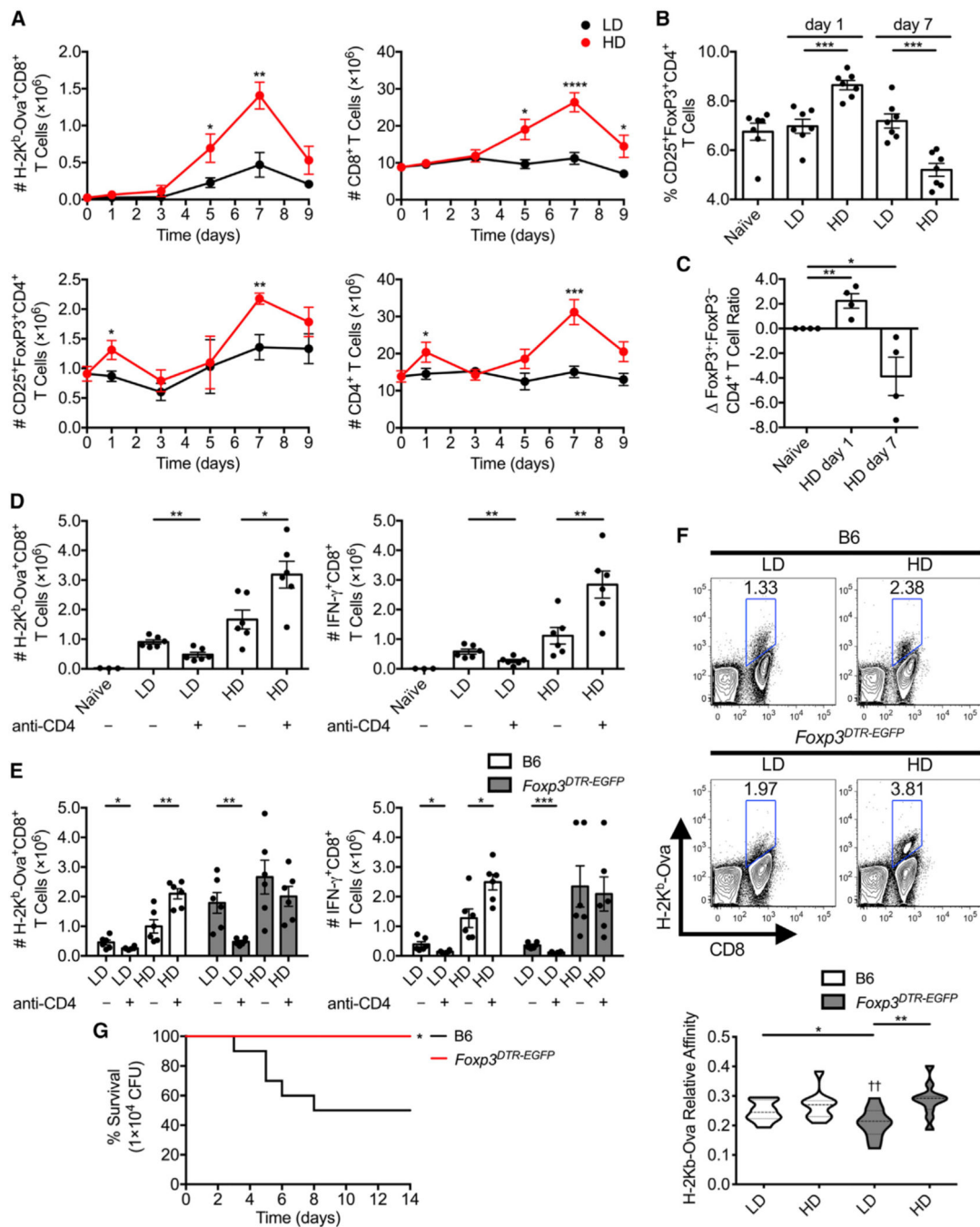


Figure 1. Induction of T Cell Responses by LD and HD *Listeria* Infection

(A–D) Groups of C57BL/6 mice systemically infected with LD or HD *Lm DactA-Ova*.

(A) Kinetics of total CD8⁺ T cells, Ova_{257–264}/H-2K^b-tetramer-binding (H-2K^b-Ova⁺) CD8⁺ T cells, total CD4⁺ T cells, and CD25⁺FoxP3⁺CD4⁺ T cells (T_{reg}) in the spleens of infected mice (n = 4–8 per group).

(B) Frequency of CD25⁺FoxP3⁺CD4⁺ T_{reg} within the total CD4⁺ T cell fraction (n = 7 per group).

- (C) Change in FoxP3⁺:FoxP3⁻ CD4⁺ T cell ratio after HD *Lm actA*-Ova infection relative to the naive cohort (D FoxP3⁺:FoxP3⁻) (n = 4 per group).
- (D) Absolute number of Ova-specific CD8⁺ T cells and Ova-specific IFN- γ ⁺ effectors at day 7 post-infection \pm CD4⁺ T cell depletion (n = 6 per group).
- (E and F) C57BL/6 and *Foxp3^{DTR-EGFP}* mice infected with LD or HD *Lm actA*-Ova with DT delivery to all animals before and throughout infection.
- (E) Absolute number of Ova-specific CD8⁺ T cells and Ova-specific IFN-g⁺ effectors at day 7 \pm CD4⁺ T cell depletion (n = 6 per group).
- (F) H-2K^b-Ova relative affinity of splenic CD8⁺ T cells calculated as the geometric mean fluorescence intensity (geMFI) of Ova₂₅₇₋₂₆₄/H-2K^b-tetramer to anti- TCR β FACS stain ratio compared between strain and *Lm* dosage (n = 10 per group).
- (G) Survival of C57BL/6 versus *Foxp3^{DTR-EGFP}* mice infected with WT *Lm* Ova, with DT injections spanning the immune response (n = 10 per group).

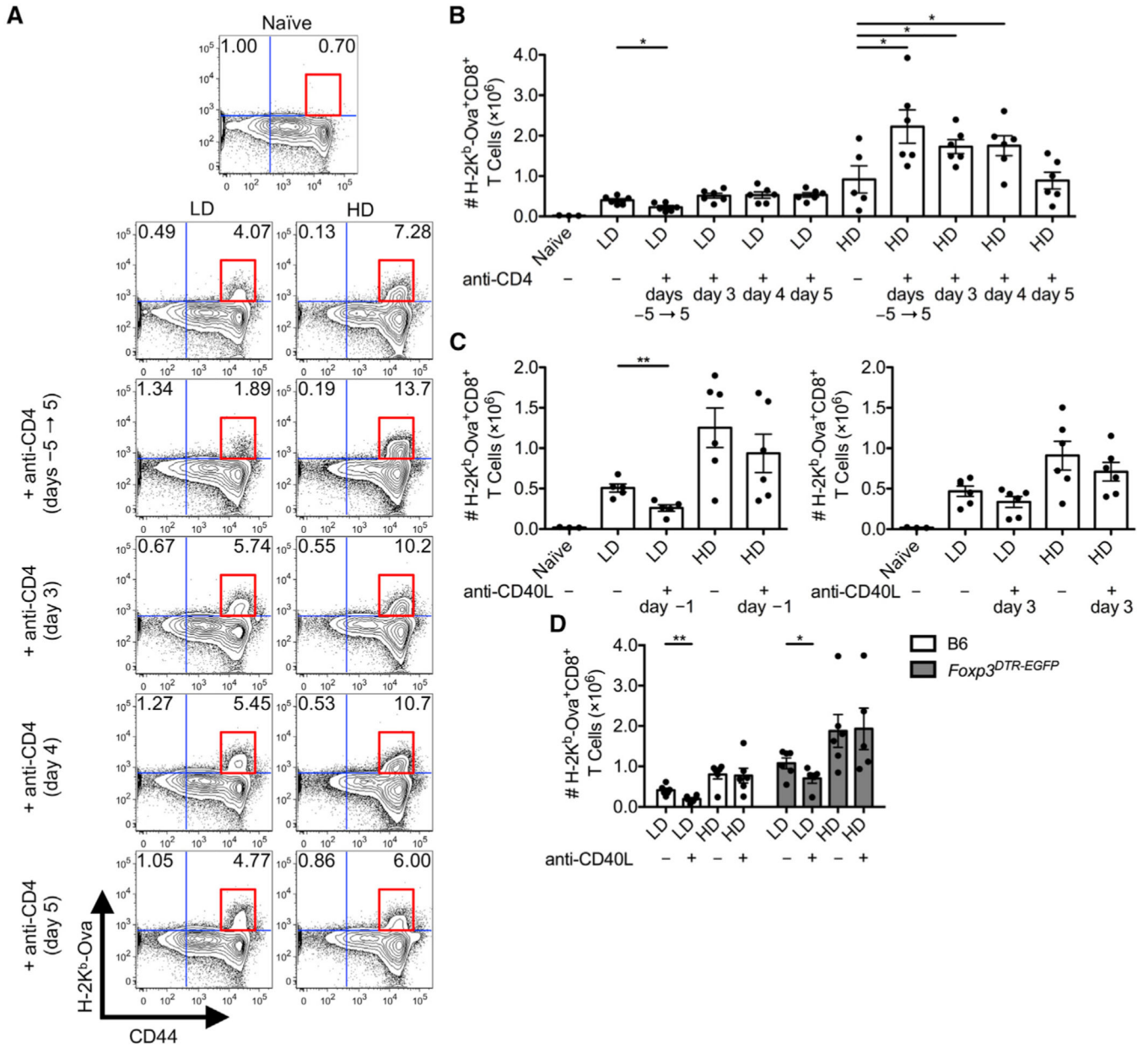


Figure 2. FoxP3⁺ T_{reg} Suppress Primary CD8⁺ T Cell Responses with a Different Kinetic Compared to T_H

(A–C) C57BL/6 mice infected with LD or HD *Lm actA-Ova*.

(A and B) (A) Frequency with CD44^{hi} inset (red box) and (B) absolute number of Ova-specific CD8⁺ T cells 7 days post-infection among total CD44^{lo-hi}CD8⁺ T cells in the spleens of mice ± CD4⁺ T cell depletion either prior to infection or at 3, 4, or 5 days post-infection (n = 5–6 per group).

(C) The absolute number of splenic Ova-specific CD8⁺ T cells at day 7 in mice that had received CD40L-blocking antibody 1 day before or 3 days after infection (n = 6 per group).

(D) C57BL/6 and *Foxp3^{DTR-EGFP}* mice i.v. infected with LD or HD *Lm actA-Ova* with DT delivery to all animals before and throughout infection. Absolute number of splenic

Ova-specific CD8⁺ T cells at day 7 in animals that had received CD40L-blocking antibody 1 day before infection (n = 6 per group).

Author Manuscript

Author Manuscript

Author Manuscript

Author Manuscript

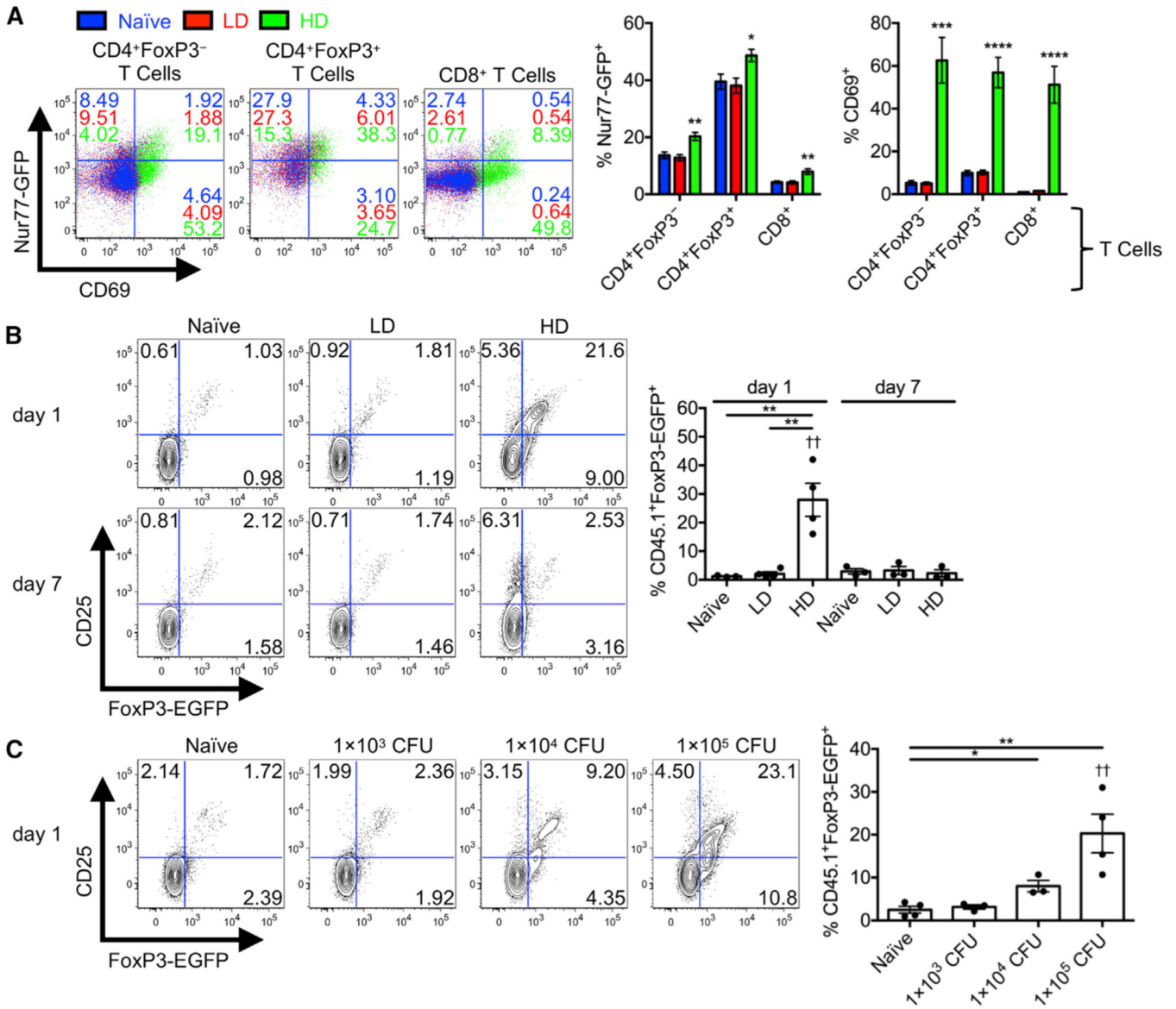


Figure 3. Inflammation-Driven Polyclonal Conversion of Conventional CD4⁺ T Cells to T_{reg}

(A) TCR engagement and surface CD69 upregulation by conventional CD4⁺ T cells (FoxP3⁻), T_{reg} (CD25⁺FoxP3⁺), and CD8⁺ T cell populations in naïve (blue) and at 24 h following LD (red) and HD (green) *Lm actA-Ova* infection of *Nr4a1^{GFP}* mice (n = 4 per group).

(B and C) Conventional CD4⁺EGFP⁻ T cells were isolated from CD45.1⁺ *Foxp3^{EGFP}* mice and transferred into C57BL/6 mice followed by a 24-h rest period. The percentage of splenic CD45.1⁺FoxP3-EGFP⁻ T cells that expressed EGFP under control of the *Foxp3* promoter (denoted as FoxP3-EGFP) after assessment of (B) LD and HD *Lm actA-Ova* day 1 (n = 3–4 per group) and 7 (n = 3 per group), as well as (C) titrated WT *Lm Ova* day 1 (n = 3–4 per group) infections.

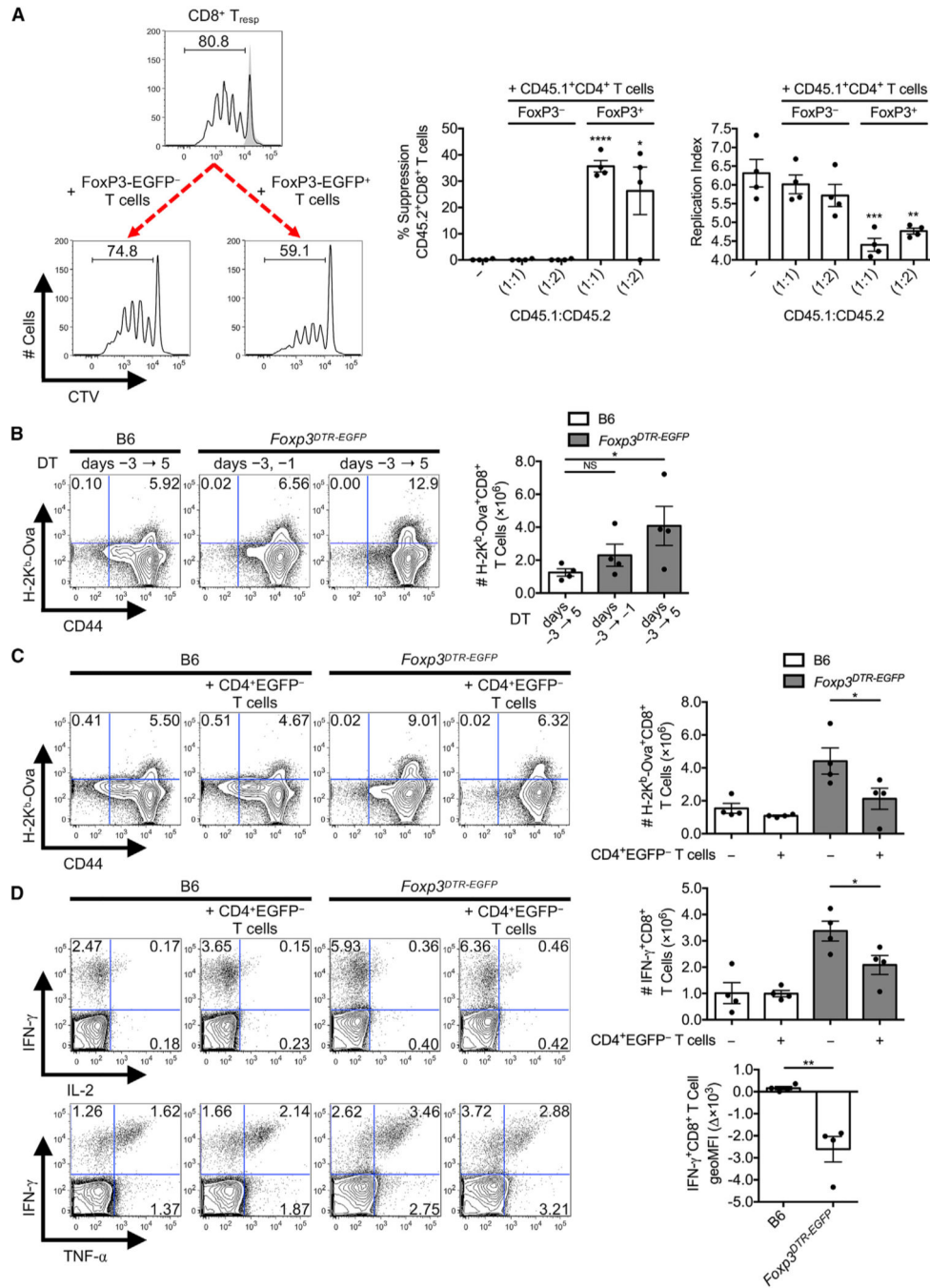


Figure 4. Converted T_{reg} Mediate Suppression of CD8⁺ T Cell Responses to *Listeria* In Vitro and In Vivo

(A) *In vitro* CD3/CD28-driven CD45.2⁺CD8⁺ T_{resp} proliferation represented as percent suppression and replication index at day 3 after co-culture of naive CellTrace Violet (CTV)-labeled CD45.2⁺CD8⁺ T_{resp} with graded populations of converted CD45.1⁺CD4⁺FoxP3-EGFP⁺ and non-converted CD45.1⁺CD4⁺FoxP3-EGFP⁻ T cells re-isolated from C57BL/6 recipient mice that underwent 24 h HD *Lm actA*-Ova infection (n = 4 per group).

(B) Absolute number of splenic Ova-specific CD8⁺ T cells at day 7 post-infection of C57BL/6 and Foxp3^{DTR-EGFP} mice infected with HD *Lm actA*-Ova. FoxP3⁺ T_{reg} depletion

was achieved via limiting DT injection to a pre-infection phase (days -3 to -1) or continuing DT administration during the immune response (days -3 to 5) (n = 4 per group). (C and D) Naive CD4⁺EGFP⁻ T cells were isolated from CD45.1⁺ *Foxp3*^{EGFP} mice and transferred into C57BL/6 and *Foxp3*^{DTR-EGFP} mice at day -1 that received a full DT regimen relative to a day 0 HD *Lm actA*-Ova infection. The frequency and absolute number of splenic (C) Ova-specific CD8⁺ T cells and (D) Ova-specific IFN-γ⁺ effectors together with change in IFN-γ production per cell ($\approx 3 \times 10^3$ IFN-γ geoMFI) at day 7 post-infection (n = 4 per group).

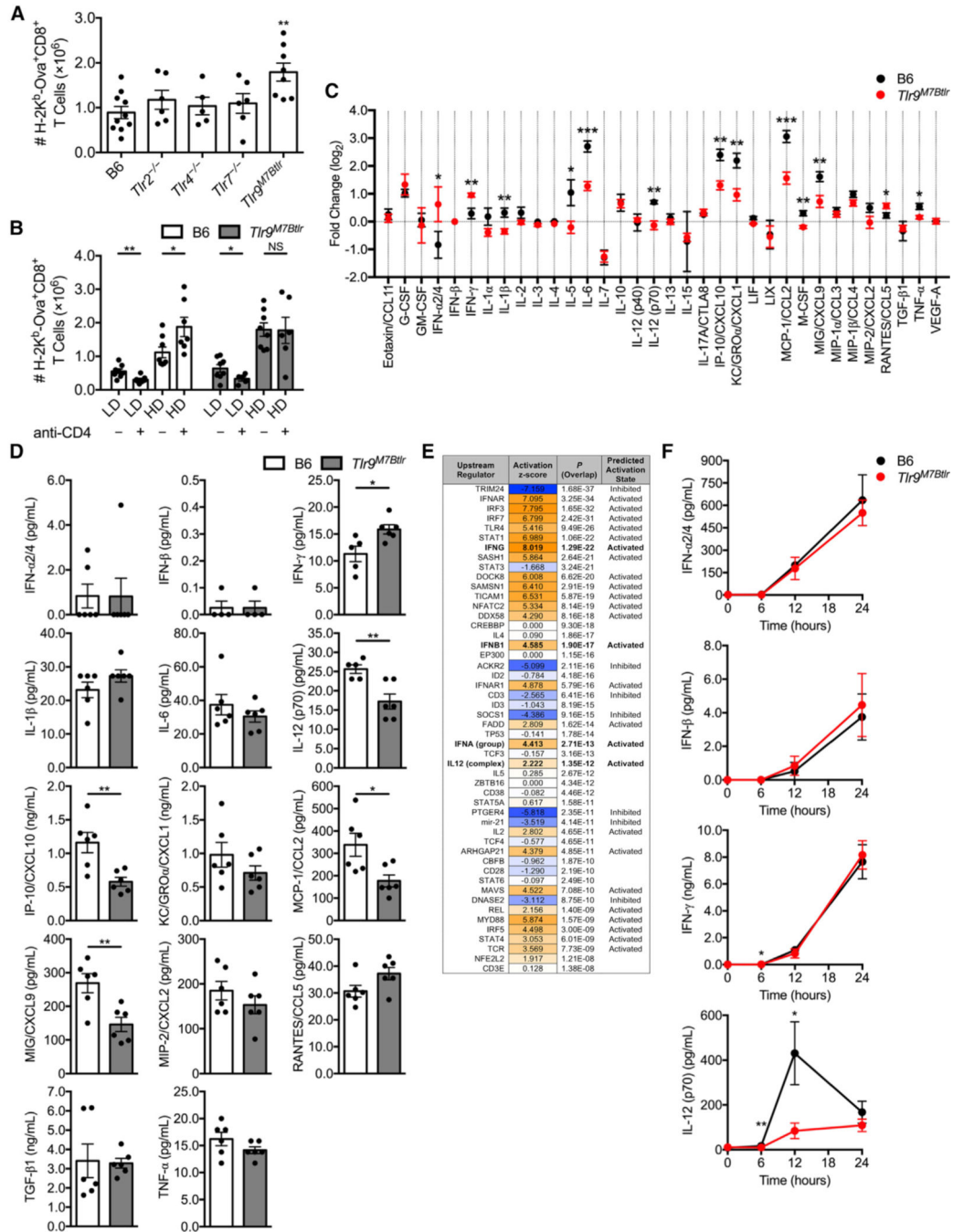


Figure 5. Role of TLR9 and IL-12 (p70) in T_{reg} Conversion

(A and B) Groups of C57BL/6 and TLR-deficient mice infected with LD or HD *Lm actA-Ova*.

(A) Absolute number of Ova-specific CD8⁺ T cells at day 7 post-infection with HD *Lm actA-Ova* compared among splenic isolates of *Tlr2*^{-/-}, *Tlr4*^{-/-}, *Tlr7*^{-/-}, and *Tlr9*^{M7Btlr} mice (n = 6–10 per group).

(B) Absolute number of Ova-specific CD8⁺ T cells at day 7 in the spleens of *Tlr9*^{M7Btlr} mice ± CD4⁺ T cell depletion (n = 6–8 per group).

(C and D) Groups of C57BL/6 and *Tlr9^{M7Btlr}* mice systemically infected with HD *Lm actA-Ova*.

(C) Fold change in serum cytokines and chemokines from 0–6 h post-infection.

(D) Selected serum cytokine/chemokine concentration at 6 h post-infection displaying significance in (C) (n = 6 per group).

(E) *Foxp3^{EGFP}* mice infected with HD *Lm actA-Ova* for 24 h. Ingenuity Pathway Analysis (IPA) upstream regulator prediction of differential gene expression profiles comparing total FoxP3-EGFP⁺ T_{reg} sorted from naive versus infected mice (top 50 significant hits; p = gene network overlap) (n = 4 per group).

(F) Kinetic display of IFN- α 2/4, IFN- β , IFN- γ , and IL-12 (p70) serum concentration in C57BL/6 and *Tlr9^{M7Btlr}* mice after exposure to HD *Lm DactA-Ova* (n = 6 per group).

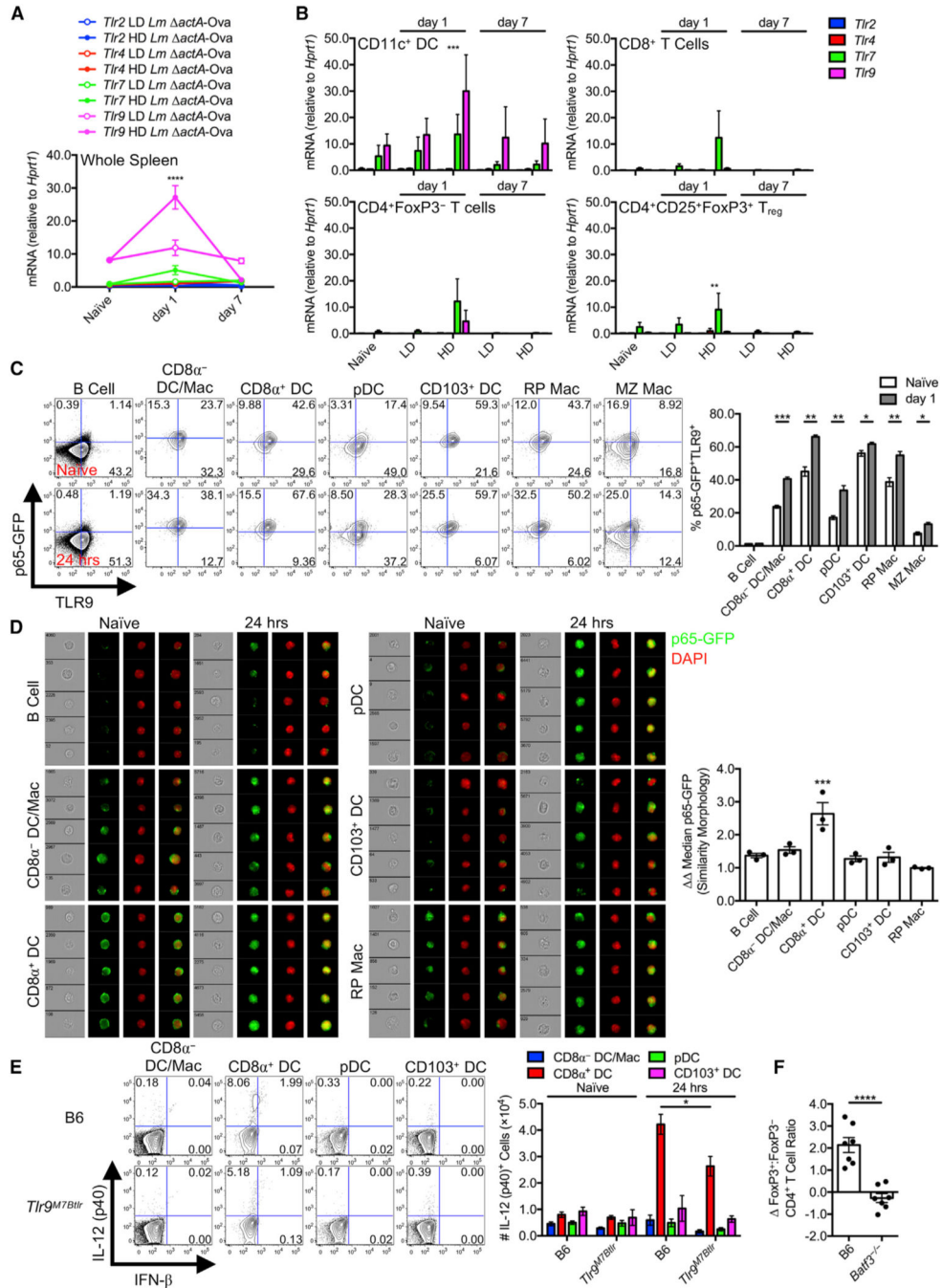


Figure 6. TLR9/NF-κB-Mediated Induction of IL-12 in CD8 α ⁺ DCs
 (A and B) *Tlr2*, *Tlr4*, *Tlr7*, and *Tlr9* mRNA normalized to *Hprt1* mRNA in (A) whole spleen and (B) sorted DC and T cell populations in C57BL/6 mice infected with LD or HD *Lm actA-Ova* (n = 3 per group).
 (C and D) p65-GFP knockin mice challenged for 24 h with HD *Lm actA-Ova*.
 (C) Frequency of p65-GFP and TLR9 expression in B cells, CD8 α ⁻ DC/Mac, CD8 α ⁺ DCs, plasmacytoid DCs (pDCs), CD103⁺ DCs, red pulp macrophages (RP Macs), and marginal zone Macs (MZ Macs) (n = 3 per group).
 (D) Microscopy images showing p65-GFP localization in the same cell types. Scale bars represent 10 μm.
 (E) Flow cytometry analysis of IL-12 (p40) production in B6 and *Tlr9*^{M7Btr} mice. The top row shows B6 mice, and the bottom row shows *Tlr9*^{M7Btr} mice. The left column shows cells stimulated with IFN-β, and the right column shows cells stimulated with *Tlr9*^{M7Btr}. The y-axis represents IL-12 (p40) expression, and the x-axis represents IFN-β expression. The percentage of IL-12⁺ cells is indicated in the plots. The bar graph shows the number of IL-12⁺ cells (x10⁶) in the spleen of B6 and *Tlr9*^{M7Btr} mice under the same conditions.
 (F) Ratio of FoxP3⁺ to FoxP3⁻ CD4⁺ T cells in B6 and *Balb/c*^{-/-} mice. The y-axis represents the ratio of FoxP3⁺ to FoxP3⁻ CD4⁺ T cells. The x-axis shows B6 and *Balb/c*^{-/-} mice.

(D) Representative ImageStream images displaying TLR9^{hi} APC subcellular localization of p65-GFP (green) and DAPI (red) and quantitative p65-GFP nuclear translocation (n = 3 per group).

(E) C57BL/6 and *Tlr9*^{M7Btlr} mice exposed to HD *Lm actA*-Ova for 24 h. Frequency and absolute number of IL-12 (p40)⁺ and IFN- β ⁺ APC subsets after PMA/ionomycin stimulation (n = 4 per group).

(F) C57BL/6 and *Batf3*^{-/-} mice infected with HD *Lm actA*-Ova for 24 h. Change in FoxP3⁺:FoxP3⁻ CD4⁺ T cell ratio at day 1 post-infection relative to the naive state (D FoxP3⁺:FoxP3⁻) (n = 7 per group).

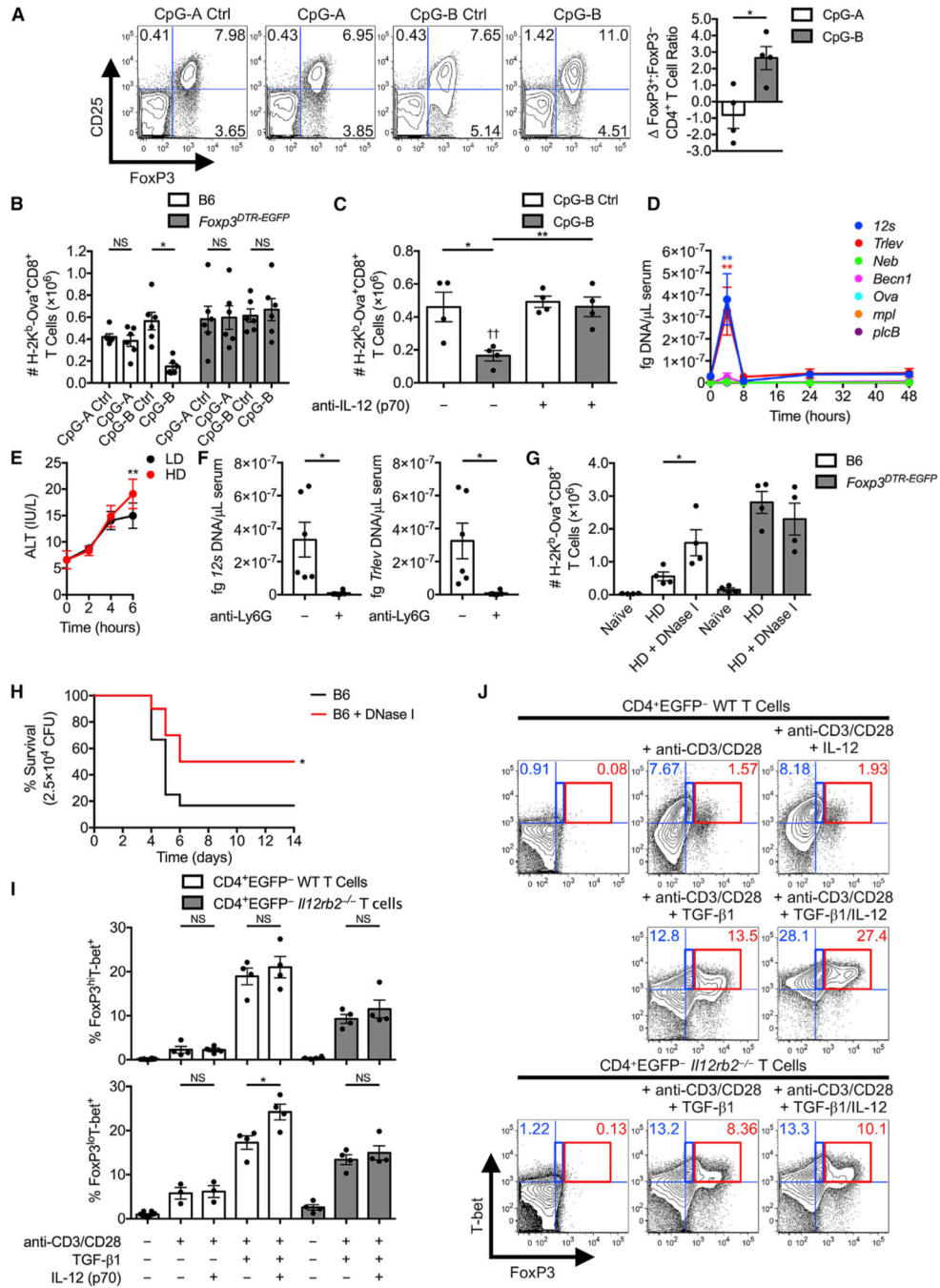


Figure 7. Release of Self-DNA Drives IL-12 (p70) Production, FoxP3 Induction, and T_{reg} Conversion from Conventional CD4⁺ T Cells
 (A) C57BL/6 mice administered 50 μg CpG-A, CpG-B, and CpG control ODNs at days -1 and 0. Frequency of splenic CD25⁺FoxP3⁺CD4⁺ T_{reg} and change in FoxP3⁺:FoxP3⁻ CD4⁺ T cell ratio relative to CpG controls (D FoxP3⁺:FoxP3⁻) at day 1 (n = 4 per group).
 (B) C57BL/6 and *Foxp3^{DTR-EGFP}* mice administered CpG ODNs as in (A) and infected with LD *Lm actA-Ova* at day 0 and co-delivered a complete DT regimen. Absolute number of splenic Ova-specific CD8⁺ T cells at day 7 post-infection (n = 6 per group).

- (C) Splenic Ova-specific CD8⁺ T cell response observed in CpG-treated or -infected C57BL/6 as in (B), with blockade of IL-12 (p70) (n = 4 per group).
- (D) Quantification of mtDNA (*12s* and *Trlev*), nDNA (*Neb* and *Becn1*), and *Lm* DNA (*Ova*, *mpl*, and *plcB*) in cell- and RNA-free serum samples after HD *Lm actA*-Ova infection of C57BL/6 mice (n = 6 per group).
- (E) Serum ALT concentration within LD versus HD *Lm actA*-Ova-infected C57BL/6 mice (n = 6 per group).
- (F) Effect of neutrophil depletion before HD *Lm actA*-Ova infection of C57BL/6 mice on mtDNA (*12s* and *Trlev*) in cell- and RNA-free serum samples isolated at 4 h post-infection (n = 6 per group).
- (G) Absolute number of splenic Ova-specific CD8⁺ T cells at day 7 post-infection in C57BL/6 and *Foxp3^{DTR-EGFP}* mice administered a complete DT regimen, systemic HD *Lm actA*-Ova, and selective DNase I delivery (n = 4 per group).
- (H) Survival of untreated versus DNase I-treated C57BL/6 mice infected with WT *Lm* Ova (n = 10–16 per group).
- (I and J) *In vitro* co-expression of FoxP3 and T-bet in conventional CD4⁺EGFP⁻ T cells isolated from *Foxp3^{EGFP}* or *Il12rb2^{-/-}Foxp3^{EGFP}* mice cultured in the presence or absence of CD3/CD28-mediated activation, rmTGF- β 1, and rmIL-12 (p70) (n = 4 per group).

KEY RESOURCES TABLE

REAGENT or RESOURCE	SOURCE	IDENTIFIER
Antibodies		
anti-CD4 (GK1.5)	Alejandro Aruffo (Bristol-Myers Squibb Pharmaceutical Research Institute, Seattle, WA) and (Noelle et al., 1992)	N/A
anti-CD4 (RM4-5) APC-eF780	eBioscience	Cat#47-0042-82
anti-CD4 (RM4-5) PerCP-Cy5.5	Tonbo Biosciences	Cat#65-0042-U 100
anti-CD8 (53-6.7) eF450	eBioscience	Cat#48-0081-82
anti-CD8 (53-6.7) PE	Tonbo Biosciences	Cat#50-0081-U 100
anti-CD11b (M1/70) PE-Cy7	3D Biosciences	Cat#552850
anti-CD11c (N418) PerCP-Cy5.5	eBioscience	Cat#45-0114-82
anti-CD25 (PC61.5) PerCP-C5.5	Tonbo Biosciences	Cat#65-0251-U 100
anti-CD40L (MR1)	Alejandro Aruffo (Bristol-Myers Squibb Pharmaceutical Research Institute, Seattle, WA) and (Noelle et al., 1992)	N/A
ant-CD44 (IM7) PerCP-Cy5.5	eBioscience	Cat#45-0441-82
ant-CD45.1 (A20) APC-eF780	eBioscience	Cat#47-0453-82
ant-CD45.2 (104) APC	Tonbo Biosciences	Cat#20-0454-U 100
ant-CD45R/B220 (RA3-6B2) APC-eF780	eBioscience	Cat#47-0452-82
ant-CD45R/B220 (RA3-6B2) BV605	BD Biosciences	Cat#563708
ant-CD69 (H1.2F3) APC	BioLegend	Cat#104513
ant-CD103 (2E7) APC	eBioscience	Cat#17-1031-80
ant-CD103 (2E7) PE	eBioscience	Cat#12-1031-82
ant-F4/80 (BM8) PE	eBioscience	Cat#12-4801-80
ant-FoxP3 (FJK-16 s) PE	eBioscience	Cat#12-5773-82
ant-GFP (pAb) FITC	Rockland Immunochemicals	Cat#600-402-215
ant-IFN- β (RMMB-1) FITC	PBL Assay Science	Cat#22400-3
ant-IFN- γ (XMG1.2) APC	eBioscience	Cat#17-7311-82
ant-IL-2 (JES6-5H4) PE	BioLegend	Cat#503808
ant-IL-4 (11B11)	BioLegend	Cat#504108
ant-IL-12 (p40) (C17.8) PE	Tonbo Biosciences	Cat#50-7123-U100
ant-IL-12 (p70) (R2-9A5)	BioXCell	Cat#BE0233
ant-Ki-67 (SolA15) eF450	eBioscience	Cat#48-5698-82
ant-Ly6G (1A8)	BioXCell	Cat#BP0075
ant-MHC II (M5/114.15.2) APC-eF780	eBioscience	Cat#47-5321-80
ant-MHC II (M5/114.15.2) eF450	eBioscience	Cat#48-5321-80
ant-NK1.1 (PK136) APC	eBioscience	Cat#17-5941-82
ant-NK1.1 (PK136) PE-Cy7	eBioscience	Cat#25-5941-82
ant-TCR β (H57-597) APC	Tonbo Biosciences	Cat#20-5961-U 100
ant-TCR β (H57-597) FITC	Tonbo Biosciences	Cat#35-5961-U 100
ant-TCR β (H57-597) Pacific Blue	BioLegend	Cat#109226
ant-TCR β (H57-597) PE	Tonbo Biosciences	Cat#50-5961-U025

REAGENT or RESOURCE	SOURCE	IDENTIFIER
ant-TCR β (H57-597) PE-Cy7	Tonbo Biosciences	Cat#60-5961-U 100
ant-TLR9 (26C593.2) AF647	Thermo Scientific and self-labeled	Cat#MA5-16178
ant-TNF- α (MP6-XT22) PE-Cy7	BD Biosciences	Cat#557644
Bacterial and Virus Strains		
WT <i>Listeria monocytogenes</i> (<i>Lm</i>) 10403S	Daniel A. Portnoy (University of California, Berkeley, CA)	N/A
WT <i>Lm</i> Ova	Daniel A. Portnoy (University of California, Berkeley, CA)	N/A
<i>Lm actA</i> 10403S	Daniel A. Portnoy (University of California, Berkeley, CA)	N/A
<i>Lm actA</i> -Ova 10403S	Daniel A. Portnoy (University of California, Berkeley, CA)	N/A
Chemicals, Peptides, and Recombinant Proteins		
CellTrace Violet (CTV)	Life Technologies	Cat#C34557
4',6-diamidino-2-phenylindole (DAPI)	Molecular Probes	Cat#D1306
diphtheria toxin (DT)	Sigma-Aldrich	Cat#D0564
DNase I, from bovine pancreas	Sigma-Aldrich	Cat#11284932001
H-2K ^b -Ova iTAG tetramer PE	MBL International	Cat#TB-5001-1
Mouse T-Activator anti-CD3/CD28 Dynabeads	GIBCO	Cat#11452D
Ova ₂₅₇₋₂₆₄ peptide (SIINFEKL)	AnaSpec	Cat#AS-60193-1
rmIL-12 (p70)	R&D Systems	Cat#419-ML-010
rmTGF- β 1	R&D Systems	Cat#7666-MB-005
Critical Commercial Assays		
human/mouse TGF- β 1 ELISA	Invitrogen	Cat#88-8350-86
liquid ALT (SGPT) Reagent set	Pointe Scientific	Cat#A7526150
live/Dead Fixable Yellow Dead Cell Stain kit	Invitrogen	Cat#L-34968
MILLIPLEX MAP 32-plex mouse cytokine/chemokine panel	EMD Millipore	Cat#MICYTMAG-7 0K-PX32
mouse IFN- α 2/4 Platinum ELISA	eBioscience	Cat#BMS6027
mouse IFN- β VeriKine ELISA	PBL Assay Science	Cat#42400
Novagen NovaQUANT Mouse Mitochondrial to Nuclear Ratio kit	EMD Millipore	Cat#72621 -1KIT
Deposited Data		
RNA-Seq metadata	NCBI gene expression omnibus	GSE106554
Experimental Models: Mice		
C57BL/6	The Jackson Laboratory	Stock#000664
<i>Act-mOva H-2kb</i> ^{-/-}	Marc K. Jenkins (University of Minnesota, Minneapolis, MN) and (Feau et al., 2011; Janssen et al., 2005)	N/A
<i>Batf3</i> ^{-/-}	The Jackson Laboratory	Stock#013755
<i>Foxp3</i> ^{EGFP} (FoxP3-EGFP)	The Jackson Laboratory	Stock#006772

REAGENT or RESOURCE	SOURCE	IDENTIFIER
<i>Foxp3</i> ^{DTR-EGFP}	The Jackson Laboratory	Stock#016958
<i>Il12rb2</i> ^{-/-}	The Jackson Laboratory	Stock#003248
<i>Nr4a1</i> ^{GFP} (Nur77-GFP)	Kristin A. Hogquist (University of Minnesota) and (Moran et al., 2011)	N/A
p65-GFP	Manolis Pasparakis (University of Cologne, Cologne, Germany) and (De Lorenzi et al., 2009)	N/A
<i>Tlr2</i> ^{-/-}	The Jackson Laboratory	Stock#004650
<i>Tlr4</i> ^{-/-}	The Jackson Laboratory	Stock#007227
<i>Tlr7</i> ^{-/-}	The Jackson Laboratory	Stock#008380
<i>Tlr9</i> ^{M7Btlr}	The Jackson Laboratory	Stock#014534
Oligonucleotides		
<i>Mus musculus Tlr2</i> QuantiTect primers	QIAGEN	Cat#QT00129752
<i>Mus musculus Tlr4</i> QuantiTect primers	QIAGEN	Cat#QT00259042
<i>Mus musculus Tlr7</i> QuantiTect primers	QIAGEN	Cat#QT00251013
<i>Mus musculus Tlr9</i> QuantiTect primers	QIAGEN	Cat#QT01043049
forward primer for <i>Lm mpl</i> CCAGTATTCGGCGGGATTGG	self-designed	N/A
reverse primer for <i>Lm mpl</i> GACCCACGCACACAGACATC	self-designed	N/A
forward primer for <i>Lm plcB</i> GCAACGGAAGACATGGTAGCAA	self-designed	N/A
reverse primer for <i>Lm plcB</i> GTAGTCCGCTTTCGCCCTTT	self-designed	N/A
forward primer for <i>Mus musculus Hpntl</i> CTCCGCCGCTTCTCTCA	self-designed	N/A
reverse primer for <i>Mus musculus Hpntl</i> ACCTGGTTCATCATCGTAATC	self-designed	N/A
forward primer for ovalbumin GTCAGCAGAGGCTGGAGTGGA	self-designed	N/A
reverse primer for ovalbumin GGCGTTGGTTGCGATGTGCT	self-designed	N/A
ODN 1585 Ctrl (CpG-A Ctrl) ggGGTCAAGCTTGAgggggg	InvivoGen	Cat#tlrl-1585c
ODN 1585 (CpG-A) ggGGTCAACGTTGAgggggg	InvivoGen	Cat#tlrl-1585
ODN 1668 Ctrl (CpG-B Ctrl) tccatgacctctgatgct	InvivoGen	Cat#tlrl-1668c
ODN 1668 (CpG-B) tccatgacctctgatgct	InvivoGen	Cat#tlrl-1668
Software and Algorithms		
Bioconductor (v3.0) package DESeq2 (v1.6.3)	Love et al., 2014	N/A
FlowJo (v9.7.5 and v10.4.2) software	Tree Star Inc.	N/A
IDEAS (v6.2.183.0) software	Amnis Inc.	N/A
Ingenuity Pathway Analysis (IPA; v01-07) software	QIAGEN	N/A
Luminex MAGPIX System with xPONENT (v4.2) software	Luminex	N/A
Python HTSeq (v0.6.0) software	Anders et al., 2015	N/A
PRINSEQ Lite (v0.20.3) software	Schmieder and Edwards, 2011	N/A
Prism (v7.0a and v8.0.2) software	GraphPad Software Inc.	N/A
SAMtools	Li et al., 2009	N/A
SoftMax Pro (v5.3b12) software	Molecular Devices	N/A

REAGENT or RESOURCE	SOURCE	IDENTIFIER
TopHat (v1.4.1) software	Trapnell et al., 2009	N/A
Other		
Cytofix/Cytoperm	BD Biosciences	Cat#554722
FoxP3 Staining set	eBioscience	Cat#00-5523-00
GolgiPlug	BD Biosciences	Cat#555029
GolgiStop	BD Biosciences	Cat#554724
ionomycin	Sigma-Aldrich	Cat#P1585
phorbol 12-myristate 13-acetate (PMA)	Sigma-Aldrich	Cat#I0634

Author Manuscript

Author Manuscript

Author Manuscript

Author Manuscript